General Disclaimer

One or more of the Following Statements may affect this Document

- This document has been reproduced from the best copy furnished by the organizational source. It is being released in the interest of making available as much information as possible.

- This document may contain data, which exceeds the sheet parameters. It was furnished in this condition by the organizational source and is the best copy available.

- This document may contain tone-on-tone or color graphs, charts and/or pictures, which have been reproduced in black and white.

- This document is paginated as submitted by the original source.

- Portions of this document are not fully legible due to the historical nature of some of the material. However, it is the best reproduction available from the original submission.

2

ER 1677

APPLICATION OF MODERATE RESOLUTION BAND MODELS TO THE PREDICTION OF HEAT TRANSFER FROM ROCKET EXHAUST PLUMES

April 1970

HAYES
INTERNATIONAL CORPORATION
BIRMINGHAM, ALABAMA

ER 1677

APPLICATION OF MODERATE RESOLUTION BAND MODELS TO THE PREDICTION OF HEAT TRANSFER FROM ROCKET EXHAUST PLUMES

April 1970

by

J. E. Reardon and G. B. McKay

This work was sponsored by the George C. Marshall Space Flight Center of the National Aeronautics and Space Administration under Contract NAS8-21162. This report along with Hayes Engineering Report No. 1678, describing the laser Doppler velocimeter development testing, constitutes the final report on the contract.

Engineering Report No. 1677

HAYES INTERNATIONAL CORPORATION
Birmingham, Alabama

ABSTRACT

Results are reviewed for a study on the application of band model representations of gaseous radiation to the prediction of heat transfer from rocket exhaust plumes. The study included development of a radiation computer program, evaluation of the effect of scale on gaseous radiations, and a radiometer measurement of a Rocketdyne J-2 engine under simulated altitude conditions.

LIST OF SYMBOLS

Symbols	Definition	Dimensions
A	Area	cm^2
a_c	Fine structure parameter for collision broadening	
a_D	Fine structure parameters for Doppler broadening	
b_c	Collision broadened line half width	cm^{-1}
b_D	Doppler broadened line half width	cm^{-1}
d	Line spacing	cm^{-1}
D	Optical depth (= -ln T)	
D*	Optical depth in the linear limit	
D_c	Optical depth for collision broadening only	
D_D	Optical depth for Doppler broadening only	
k	Linear absorption coefficient	cm^{-1}
k(STP)	Linear absorption coefficient at standard temperature and pressure	cm^{-1} atm^{-1}
L	Upper limit of path length	cm
N_ω^o	Blackbody radiance	watts/cm-ster
p	Pressure	atm
$\dot{q}$	Heat transfer rate	watts
R	Radial coordinate in gas property data	cm
s	Dimension along line of sight	cm
T	Temperature	^oK
U	Coordinate defined in Figure 1	cm
V	Coordinate defined in Figure 1	cm
W	Coordinate defined in Figure 1	cm
X	Coordinate defined in Figure 1	cm
Y	Coordinate defined in Figure 1	cm

LIST OF SYMBOLS (Continued)

Symbols	Nomenclature	Dimensions
Z	Coordinate defined in Figure 1	cm
Δ	Integration interval prefix	
η	Angular coordinate in three-dimensional property data	degrees
θ	Spherical elevation angle in Figure 1	degrees
T	Transmissivity	
ϕ	Spherical azimuth angle in Figure 1	degrees
ω	Wavenumber	cm^{-1}
Ω	Angle of inclination of the surface normal shown by Figure 1b	degrees

Subscripts

f	Final value
i	Initial value or species
o	Full scale condition
p	Coordinate of the point to which radiant heat transfer is being calculated
STP	Standard temperature and pressure

TABLE OF CONTENTS

1 INTRODUCTION

Radiation from rocket exhaust plumes produces significant heating loads on the base region of rocket vehicles and surrounding launch structures. As a result of the concern over the accurate prediction of this radiation, Marshall Space Flight Center has sponsored the development of advanced methods of evaluating radiant transfer from inhomogeneous gases. The methods developed used small spectral intervals (25 cm^{-1}) and were proven to be quite accurate under laboratory conditions, but several problems remained.

The quantity of data required to describe a complex inhomogeneous gas, such as a three-dimensional rocket exhaust plume, plus the spectral data for the radiation calculation proved to be a storage problem for the computers which were available, and computation time was rather long. In addition, there was the problem of accurately predicting the gas properties of a rocket plume. The methods used for predicting rocket exhaust plumes could not accurately account for effects which occured in rocket nozzles such as non-uniform injection of propellants, injection of turbo pump exhaust into the nozzle boundary layer, and the occurance of carbon particles when kerosene was the fuel.

The work under this contract was directed primarly at developing an advanced radiation computer program which was more flexible in operation than previous programs and evaluating methods of reducing the required computation time. A study was also made to evaluate the possibility of scaling gaseous radiation to assist in evaluating cases in which it is difficult to analytically estimate the gas properties. In addition to this analytical work, a radiometer measurement was made on a J-2 engine operating under simulated altitude conditions to compare with the radiation prediction methods.

This report describes the radiation computer program, scaling study, and radiation measurement, and includes recommendations for further work in improving heat transfer estimates from rocket exhaust plumes.

Acknowledgement is made to Linda White and other personnel of Computer Sciences Corp. at the MSFC Computation Laboratory who assisted in programming and documentation of the radiation computer program.

2 RADIATION COMPUTER PROGRAM

A radiation computer program was developed during this study to predict the heat transfer from rocket exhaust plumes. The program uses a random (or statistical) band model representation for water vapor, carbon dioxide and carbon monoxide and also includes an absorption only (no scattering) representation for small carbon particles. The program is an improvement of those described in references 1 and 2 with increased capabilities and operating flexibility.

The program is available by request through the Thermal Environment Branch of the Aero-Astrodynamics Laboratory (S&E-AERO-AT) at the Marshall Space Flight Center. The documentation furnished with the program gives detailed instructions for operation, so the description here will be of a general nature, pointing out the characteristics of the program and describing the results of some methods used to reduce the program running time. First, the general program arrangement and operating procedure will be presented to indicate the overall scope and capability of the program, then separate discussions will be presented of the program geometry for gas property interpolation and the radiation calculation procedures. Finally, the results of increasing integration step size to reduce computation time will be reviewed.

2.1 Program Arrangement

The program arrangement was chosen to provide integration of the radiation heat transfer equation with increased flexibility and reduced computer storage limitations in comparison with earlier programs.

The heat transfer equation which is integrated by the program is

$$q/A = \int_{\theta_i}^{\theta_f} \int_{\phi_i}^{\phi_f} \int_{0}^{L} \int_{\omega_i}^{\omega_f} -N_{\omega}^{o}(dT/ds)\, ds\, d\omega\, d\phi\, \cos\theta\, \sin\theta\, d\theta \qquad (2.1)$$

with the geometry shown in Figure 1. The program performs the integration numerically using input values of integration limits, integration step size, and gas properties. First, a tape is prepared with the gas properties along each line of sight, then the properties are read back and the radiation along each line of sight is calculated and summed to give the irradiance.

The two groups of data which require a large amount of computer memory are the gas properties and the absorption coefficients. These groups are separated by having two groups of overlay subroutines for handling the flow field (gas property) interpolation and the radiation calculation. The arrangement of these subroutine groupings with the origin for the overlays is shown schematically in Figure 2.

The interpolation (FLOW) subroutines can perform various modifications on the flow field in addition to performing the gas property interpolation. Gas properties may be input from cards or tape. The input properties may be transferred to another tape if desired after being modified by scaling or adding carbon. The tape format used for the axisymmetric flow field input is compatible with the tapes prepared by the JUGGLE subroutine of the method of characteristics program described in reference 3. The format for the three-dimensional flow field is similar, but no program is currently available to generate a three-dimensional flow field, so these must be assembled manually.

The flow field properties may be input in either metric or English units, but the program will convert the English units and perform all calculations in the metric system and then reconvert to English units for output. If a change in units or other properties are desired, scale factors are provided to multiply the input values. An additional option for adding carbon to the flow field is provided since the gas property tapes prepared by the method of characteristics program (reference 3) do not contain the correct carbon concentration for kerosene/oxygen propellants. This is caused by the inability of the theoretical equilibrium chemistry used by the program to predict the production of carbon in greater than equilibrium quantities. The radiation calculation, or RAD group of subroutines provide for modification and output of absorption coefficient and line density data, prediction of radiation using Model 3A or Model 3 (to be described later), and printed and plotted output of spectral data. The coefficient data may be modified by scaling or reading new input data to replace the values stored in the block data statements. The scaling factors are not normally required and were provided primarily to evaluate the sensitivity of the predicted radiation to variations in the coefficient data. The ability to modify the absorption coefficients is also not normally used, but it is sometimes required. For example, to provide a finer spectral definition of carbon dioxide, absorption coefficients at smaller spectral intervals may be loaded, or if the Model 3 radiation calculation is used, the carbon dioxide line density data must be modified.

The spectral output provides the spectral irradiance in a variety of units, and if a detailed study of the characteristics of a single line of sight is desired, the transmissivity, optical depth, and optical parameters of each gas can be provided. Plotted output of the same parameters are available as a function of either wavelength or wavenumber.

2.2 Gas Property Interpolation

Tabulated gas property data are input to the program in a cylindrical coordinate system. In the case of an axisymmetric property variation, the position variables are simply axial position (Z) and radius (R). The three-dimensional property specification is not so straightforward since variations to be described later are used to take advantage of symmetry in the flow field for reducing the quantity of input data. But, even with these variations, the property data for three-dimensional flow fields uses at a basically cylindrical system with property data input as a function of axial position (Z), angle (η), and radius (R).

During the interpolation procedure, the basic coordinate system used is a Cartesian system, XYZ, with the Z-axis identical with the central axis of the gas property data. The UVW coordinate system, in which the heat transfer equation is integrated, can be located relative to the XYZ system by either of two methods. In both cases, the origin of the UVW system, the point to which the heat transfer is being calculated, is located by its coordinates (X_p, Y_p, Z_p). For the more general case, the orientation of the UVW axes is specified by nine direction cosines defining the relative angle of each of the U, V, and W axes with respect to the X, Y, and Z axes. Since in many cases, the surface of interest is normal to a plane containing the Z axis, a simplified procedure was adopted for this case. This procedure, illustrated in Figure 1b, requires only the inclination angle, Ω, of the surface normal relative to a vector parallel to the Z axis ($\vec{z}$), but this method must be restricted to cases in which the Z-axis is in the U-W plane.

The axisymmetric gas properties are specified at arbitrary values of Z, and at each of these Z-cuts the radius, temperature, pressure, and species mole

fractions are specified at arbitrary spacing from the Z-axis (R = 0) to the outer boundary of the gas. There is no limit to the number of Z-cuts which can be used since the program will load the property data up to its capacity, generate the initial data along the lines of sight, then read in successive sections of the property data and add to the lines of sight until the problem limits have been reached.

As stated earlier, the system for specifying the property data for three-dimensional property variations does not necessarily use a cylindrical system about the Z-axis. Two additional parameters are provided, CTCD and HANG, to allow simplier definition of the property values in the case of rocket engine clusters. The range of η over which radial property data are required for various values of the engine center to center distance (CTCD) and symmetrical sector half angle (HANG) are illustrated in Figure 3. The options used for clustered engines greatly reduce the handling and storage problem for the property data.

It should be noted that the arrangement illustrated in Figure 3 in which the symmetry is assumed between the center and outboard engines about a plane at CTCD/2 is not technically correct. Although the gas properties about the impingment plane between the engines are initially symmetrical, variations will exist downstream due to different conditions which will develop as the shocks from the impingement zones move toward the engine centerline. In spite of this, the configuration shown by Figure 3c is compatible with the present approximate methods of estimating exhaust plume characteristics for clusters of rocket engines and will be useful until more exact methods are available.

The method of interpolating in the gas property data to get the property data along each line of sight is basically a linear method, but it differs slightly

from the procedure used in previous programs. The interpolation between Z-cuts is carried out along a line at a constant percentage of the radius rather than parallel to the Z-axis. This new method gives a more realistic estimate of rocket exhaust plume properties particularly in regions near the plume boundary.

Another feature which has been added to this program to provide more accurate interpolation is the shock option. When this option is used, data on the location of shocks in the gas are specified so the interpolation procedure will only take data from the proper side of the shock. This allows a sharp discontinuity when the shock is reached by a line of sight rather than having a more gradual change in temperature caused by interpolating between a high temperature at one Z-cut and a low temperature at the other.

Provision for blockage of lines of sight by solid objects is simulated in the same manner as in the programs of references 1 and 2. This consists of up to 50 circles which can be located anywhere in the X, Y, Z coordinate system, but the plane of the circle must be parallel to the X-Y plane. Each circle is located by its center coordinates and radius, and the type of blockage is defined as either a "disk" or a "hole". The "disk" blocks any line of sight which passes within its radius while the "hole" blocks lines of sight which pass in its plane outside of its radius.

Additional features of the program geometry include options for varying the integration interval for the line of sight distance, s, and the azimuth angle, ϕ, to reduce the problem integration time. These features will be described along with a spectral integration interval study in Section 2.4.

2.3 Radiation Analysis

The general method of analysis, referred to here as the band-model prediction method, uses absorption coefficients corresponding to the thin-gas values. These absorption coefficients are used with a random (or statistical) band-model representation of the curve of growth. The effective fine structure parameters for both Doppler and collision broadening are evaluated using a modified Curtis-Godson approximation. In this section, the equations used will be presented with a brief summary of the sources of the data which are used for water vapor, carbon dioxide, carbon monoxide, and carbon particles. In addition, the table system used for storing the data in the program will be outlined.

The radiant flux is calculated using equation 2.1 in a spherical coordinate system centered at the point of interest (Figure 1). In this system, the inclination of a line of sight, s, to the surface normal, W, is the angle, θ, while the angle between the projection of s in the U-V plane and the U axis is ϕ. When equation 2.1 is put in numerical form, it becomes

$$\dot{q}/A = \sum_{\theta_i}^{\theta_f} \sum_{\phi_i}^{\phi_f} \sum_{\omega_i}^{\omega_f} \sum_{0}^{L} -N_{\omega}^{o}\left[\bar{T}(s,\omega) - \bar{T}(s-\Delta s,\omega)\right] \cos\theta \sin\theta \, \Delta\theta \, \Delta\theta \, \Delta\omega. \tag{2.2}$$

This is evaluated using the average transmission over a spectral interval $\Delta\omega$.

$$\bar{T}(s,\omega) = \exp\left[-\bar{D}(s,\omega)\right] \tag{2.3}$$

where the optical depth, $\bar{D}(s,\omega)$, is summed over the i radiating species

$$\bar{D}(s,\nu) = \sum_i \bar{D}(s,\omega, i). \qquad (2.4)$$

The details of the evaluation of the optical depth vary depending upon the radiating species considered, and will be described below. In the following description, the functional notation for position, s, wavenumber, ω, and species, i, will be omitted except where required for clarity.

The carbon particles in the rocket exhaust are treated as a gas since they have been shown to be so small that scattering can be neglected without appreciable error for a total radiation calculation (references 4 and 5). With this assumption, the optical depth for carbon particles is simply

$$\bar{D} = \int_0^s \bar{k}(T)\, \rho ds', \qquad (2.5)$$

where $\bar{k}$ (T) is the linear absorption coefficient per unit density and path length, and ρ is the local carbon density.

The absorption coefficients for carbon particles were determined by a combined analytical and experimental technique described in reference 4. This determination provided data over the ranges of 1 to 4μ in wavelength and 300°K to 2600°K in temperature. Since an appreciable amount of heat transfer could occur outside of the 1 to 4μ spectral range, the data was extended as described in reference 6. The extension used a combination of the analytical data of reference 3 for short wavelengths (<1μ) and lower temperatures (<1600°K) and an extrapolation for the larger wavelengths (>4μ) and higher temperatures (>1600°K). With this extension, carbon absorption coefficients are available in the program over a range of wavenumbers from 10^3 cm^{-1} to 2×10^4 cm^{-1}. Since the carbon absorption coefficients are continuous over the spectrum they are represented for

computational purposes by fourth order polynomials in wavenumber for seven different temperatures. In the computer program, the coefficient for any particular spectral interval is then taken to be the coefficient at the center of the wavenumber interval.

The optical depth for each of the gaseous constituents is a function of the analytical model chosen. In the development of the analysis of the gaseous radiators (7) through (10), two analytical models were recommended. The theoretically more exact method, Model 3, uses a number of line groups for each species to account for "hot lines" from high temperature regions which are not significantly attenuated when passing through lower temperature regions. From this model, a simplified model was developed in which all the lines for each species are grouped together. This is termed Model 3A. A comparison of the equations used in determining the optical depth for Model 3 and Model 3A is presented in Table 2.1. Although Model 3 is shown as an infinite sum of line groups, four or five groups should be sufficient in most applications, and a total of ten line groups is all that is allowed in the program. In actual practice, Model 3 will seldom be used for heat transfer calculations. The primary reason for providing this model in the program is to allow an evaluation of Model 3A by comparing the two methods over small regions. In the cases which have been checked for rocket exhaust plumes, Model 3 generally predicts slightly less radiation than Model 3A, and there is no evidence that Model 3 is actually more accurate even though it is theoretically more exact.

The effect of inhomogeneous gas properties on the fine structure parameters ($\bar{a}_C$ and $\bar{a}_D$) is accounted for by the use of a modified Curtis-Godson approximation. In this application, the approximation is modified in the sense that it

TABLE 2.1
COMPARISON OF MODELS 3 AND 3A

PARAMETER	MODEL 3	MODEL 3A
OPTICAL DEPTH	$D = \sum_{n=0}^{\infty} D_n$	$D = \sqrt{1-Y^{-1/2}}\ D^*$ (2.6)
OPTICAL DEPTH OF THE nth LINE GROUP	$D_n = \sqrt{1-Y_n^{-1/2}}\ D_n^*$	NOT APPLICABLE (2.7)
COMBINED COLLISION AND DOPPLER OPTICAL DEPTHS	$Y_n = \left[1-\left(\frac{D_{cn}}{D_n^*}\right)^2\right]^{-2} + \left[1-\left(\frac{D_{Dn}}{D_n^*}\right)^2\right]^{-2} - 1$	$Y = \left[1-\left(\frac{D_c}{D^*}\right)^2\right]^{-2} + \left[1-\left(\frac{D_D}{D^*}\right)^2\right]^{-2} - 1$ (2.8)
OPTICAL DEPTH FOR THE WEAK LINE (LINEAR) LIMIT	$D_n^* = \int_0^s \bar{k}_n\, ds'$	$D^* = \int_0^s \bar{k}(p_i, T)\, ds'$ (2.9)
OPTICAL DEPTH FOR A PURE COLLISION CURVE OF GROWTH	$D_{c_n} = D_n^* \left(1 + D_n^*/4\bar{a}_{c_n}\right)^{-1/2}$	$D_c = D^* \left(1 + D^*/4\bar{a}_c\right)^{-1/2}$ (2.10)
OPTICAL DEPTH FOR A PURE DOPPLER CURVE OF GROWTH	$D_{D_n} = 1.7\,\bar{a}_D \sqrt{\ln\left[1+\left(\frac{0.589 D_n^*}{\bar{a}_{Dn}}\right)^2\right]}$	$D_D = 1.7\,\bar{a}_D \sqrt{\ln\left[1+\left(\frac{0.589 D^*}{\bar{a}_D}\right)^2\right]}$ (2.11)

TABLE 2.1 (Continued)
COMPARISON OF MODELS 3 AND 3A

PARAMETER	MODEL 3	MODEL 3A	
COLLISION BROADENED FINE STRUCTURE PARAMETER	$\bar{a}_{c_n} = \frac{1}{D_n^*} \int_0^s \frac{b_c}{d_n} \bar{k}_n ds'$	$\bar{a}_c = \frac{1}{D^*} \int_0^s \frac{b_c}{d} \bar{k}(p_i, T) ds'$	(2.12)
DOPPLER BROADENED FINE STRUCTURE PARAMETER	$\bar{a}_{D_n} = \frac{1}{D_n^*} \int_0^s \frac{b_D}{d_n} \bar{k}_n ds'$	$\bar{a}_D = \frac{1}{D^*} \int_0^s \frac{b_D}{d} \bar{k}(p_i, T) ds'$	(2.13)
ABSORPTION COEFFICIENT FOR THE nth LINE GROUP	$\bar{k}_n = \bar{k}(p_i, T) \frac{f_n \exp(-\theta n/T)}{\sum_{n=0}^{\infty} f_n \exp(-\theta n/T)}$ f_n / θ(°K) H_2O: 1.0 / 2300 CO_2: 1.0 / 960 CO: 1+n / 3123	NOT APPLICABLE	(2.14)
BAND AVERAGED ABSORPTION COEFFICIENT (CM^{-1}). THE COEFFICIENT AT STANDARD TEMP. AND PRESS. $\bar{k}$ (STP), IS TABULATED AS A FUNCTION OF WAVENUMBER AND TEMPERATURE.	$\bar{k}(p_i, T) = \bar{k}(STP)(p_i/1 atm.)(273/T)$		(2.15)

TABLE 2.1 (Continued)
COMPARISONS OF MODELS 3 AND 3A

PARAMETER	BOTH MODELS 3 AND 3A
COLLISION HALF-WIDTH (CM^{-1}) FOR THE ith SPECIES. BROADENING SPECIES NOTED BY j. PARTIAL PRESSURES p_i and p_j ARE IN ATMOSPHERES, AND THE TEMPERATURE T IS IN ^{o}K.	$$b_{c_i} = \sum_j \left[(b_{i,j})_{STP} \, p_j \left(\frac{273}{T}\right)^{\eta_{i,j}} \right] + (b_{ii})_{STP} \, p_i \left(\frac{273}{T}\right)^{\eta_{ii}} \quad (2.16)$$

i	j	$(b_{ij})_{STP}$	η_{ij}	$(b_{ii})_{STP}$	η_{ii}
H_2O	H_2O	(0.09)	0.5	0.44	1.0
	N_2	0.09			
	O_2	0.04			
	H_2	0.05			
	CO_2	0.12			
	CO	0.10			
CO_2	CO_2	0.09			
	H_2O	0.07			
	N_2	0.07			
	O_2	0.06			
	H_2	0.08			
	CO	0.06			
CO	CO	0.05			
	H_2O	0.05			
	CO_2	0.05			
	H_2	0.05			
	N_2	0.05			
	O_2	0.05	0.5		

DOPPLER HALF-WIDTH (CM^{-1})	$$b_{D_i} = (5.94 \times 10^{-6}) \frac{\omega}{m_i^{1/2}} \left(\frac{T}{273}\right)^{1/2} \quad (2.17)$$ WHERE m_i = MOLECULAR WT. OF THE ith SPECIES

TABLE 2.1 (Concluded)

COMPARISONS OF MODELS 3 AND 3A

PARAMETER	MODEL 3	MODEL 3A
LINE DENSITY (CM)	$1/d_n = g_n/d_o$	
	SPECIES: H_2O; g_n: 1; $1/d_o$: SEE NOTE BELOW	FOR H_2O
	SPECIES: CO_2; g_n: $(1+\epsilon n)^2$; $1/d_o$ AND ϵ TABULATED FOR ω, T	1/d is tabulated as a function of ω and T, but an approximate mathematical expression is $1/d = EXP[\ 0.7941\ SIN\ (0.0036\omega - 8.043) + D(T)]$
	SPECIES: CO; g_n: 1; $1/d_o$: 0.29	Where $D(T) = -2.295 + 0.3004 \times 10^{-2}\ T - 0.366 \times 10^{-6}\ T^2$
	FOR H_2O $1/d_o = 1/d\ \frac{(1-EXP(-\theta/2T))}{(1+EXP(-\theta/2T))}$	FOR CO_2
	WHERE 1/d IS DETERMINED AS IN MODEL 3A	1/d IS TABULATED AS A FUNCTION OF ω AND T
		FOR CO $1/d = 1/d_o\ \frac{(1+EXP(-\theta/2T))^{1.75}}{(1-EXP(-\theta/2T))}$

is applied to a spectral interval rather than a single spectral line. Experimental evidence of the validity of this modification of the Curtis-Godson approximation has been presented in references 9, 10, and 11.

The band model parameters used in the program were obtained both experimentally and theoretically. Collision-broadened line half-widths, b_C, were obtained from approximate analytical expressions (equation 2.16) with coefficients based on experimental or theoretical data in most cases (reference 8), but where no data were available, estimates were made. The evaluation of the Doppler-broadened line half-width, b_D, was more straight forward, and resulted in a theoretical expression as a function of wavenumber, molecular weight, and temperature (equation 2.17). Values of $\bar{k}$ (STP) and 1/d used in the program for H_2O were calculated from experimental data as described in reference 10, and the additional values of f_n and g_n used in Model 3 were assumed to be 1 (reference 8). Further theoretical studies (9) have indicated that both g_n and f_n tend to increase with n, but no revised expressions have been recommended. The values of $\bar{k}$ (STP), 1/d, f_n, and g_n used in the program for CO_2 and CO were evaluated from theoretical calculations by Malkmus and Thomson (12) through (17), and in the case of CO_2, many of these theoretical calculations have been verified by experiments.

Values of $\bar{k}$ (STP) and 1/d are stored in a large table in the program as a function of table entry number and temperature. Space is provided for seven temperature values and 1200 table entries. Variables, subscripted to denote the particular species, are used to assign temperatures to the table section for each species and to relate the table position to a particular species and spectral position. This allows flexibility in modifying the data in the table with minor program changes.

As presently configured, the table contains the following data:

Constituent	Parameter	Position in Table	Wavenumber Range, cm^{-1}	Temperature, ^{o}K
H_2O	$\bar{k}$ (STP)	1-439	50-11000	300,600,1000,1500,2000,2500,3000
	$1/\bar{d}$ (STP)	440-878		
CO_2	$\bar{k}$ (STP)	879-1009	500-3750	300,600,1200,1500,1800,2400,3000
	$1/\bar{d}$ (STP)	1010-1140		
CO	$\bar{k}$ (STP)	1141-1194	1025-2350	300,600,1200,1800,2400,3000,5000.

All the spectral data is provided at 25 cm^{-1} intervals, but data for CO_2 is available at smaller intervals in references 7 and 8. The CO_2 table could be modified using these data to give a smaller spectral interval for calculations using CO_2 only. But the program has no provision for interpolating between the entries for H_2O and CO, so 25 cm^{-1} is the smallest interval that can be used for a multi-constituent problem with the programmed data.

The line density for CO is defined mathematically as shown in Table 2.1, and provision is made in the program for determining the line density for H_2O using either the tabulated data or the mathematical approximation from reference 10 as shown in Table 2.1. This mathematical definition can be used in place of the tabulated values by exercising an input option, or a permanent change can be made in the program to save table space by a simple change in the block data statements containing the tabulated values of 1/d.

In preparing the tables for the program, it was necessary to assign values for some parameters without satisfactory theoretical justification since any reasonable value would be better than zero in cases where no data were available. In the case of H_2O, the tabulated data provided for 1/d in reference 10 did

not include an entry at 300°K and only covered a range of 1150 to 7500 cm^{-1}, so the mathematical approximation described earlier was used to fill in the table. The absorption coefficients provided in reference 10 only cover a range of 50 to 9300 cm^{-1}, so values from reference 7 were used from 9325 to 11000 cm^{-1}.

The extent of the data added for CO_2 to complete the tables depended upon the band, so each band will be described separately. In the 2.7μ band (3000 - 3770 cm^{-1}) absorption coefficients were provided in reference 7 with 5 cm^{-1} and 10 cm^{-1} spacing for temperatures from 300°K to 3000°K. These data were interpolated to get data at 25 cm^{-1} intervals from 3000 cm^{-1} to 3750 cm^{-1}. The range over which 1/d was provided in reference 8 was more limited. It had a lower limit of 3080 cm^{-1} and only had temperatures through 1800°K. Since the tabulated values given did not change as a function of wavenumber in the lower range, the values from 3000 cm^{-1} to 3075 cm^{-1} were taken as equal to those below 3150 cm^{-1} in the table. The values of 1/d for temperatures above 1800°K have been taken as equal to those at 1800°K until additional data is available.

In the 4.3μ band (1900 - 2395 cm^{-1}) complete data are provided in references 7 and 8 for k and 1/d at intervals of 5 cm^{-1}. These were interpolated to provide tabulated data for the program at 25 cm^{-1} intervals from 1900 cm^{-1} to 2375 cm^{-1}.

In the 15μ band (500 - 880 cm^{-1}) k was given by reference 7 for temperatures up to 2400°K at 5 cm^{-1} intervals, but no values for 1/d were provided by reference 8. The 2400°K values for k from reference 7 were also used for 3000°K in the data table to maintain a consistent table, but radiation at 15μ for a 3000°K gas temperature would not be significant compared to that at shorter wavelengths. Values of 1/d at 15μ were estimated as a function of temperature from

the data in reference 15, but no wavenumber dependency is given.

The values of absorption coefficients for CO were taken directly from reference 7 and no modification or additions were required.

2.4 Integration Interval Considerations

If the radiation computer program is used with geometric integration intervals small enough to define the gas variations well and with the minimum 25 cm^{-1} spectral integration interval, the computation time for most applications would be excessive. Therefore, program options have been provided in the integration of equation 2.2 to give flexibility in varying the geometric intervals (Δs and $\Delta\phi$), and a study has been made of averaging methods which may be used to obtain larger spectral intervals ($\Delta\omega$). Unfortunately, there is no quantitative guide that can be used in applying the larger integration intervals, so each problem must be evaluated based on past experience and the characteristics of the problem. In this section the logic used in increasing the integration intervals will be presented along with some examples of the results which have been obtained.

Line of Sight Interval - Δs

The only integration interval which has an evaluation of its size based on the problem variables built into the program is the interval along the line of sight, Δs. This interval can be controlled by a temperature step, ΔT, so that an integration step in equation 2.2 is taken only when a specified value of temperature difference has been reached. This allows a small value of Δs to be used in searching the gas properties to accurately define the variations, without wasting integration

time in regions of relatively uniform temperature. When an integration step is computed, it uses the arithmetic average of the properties at the Δs intervals over the larger temperature interval.

Evaluation of the errors caused by using the ΔT integration interval is not straightforward since both the error and time saved depend upon the value chosen for Δs. But experience with rocket exhaust plume calculations indicates that computation time can be reduced more than 50 percent with less than one percent loss in accuracy by using temperature intervals of 50 to 100°K with Δs intervals of 5 to 10 cm. The best procedure for a particular problem is to select a typical line of sight with severe property variations and evaluate the precision obtained with various values of ΔT and Δs.

Angular Interval-$\Delta\phi$

Ability to vary the spherical azimuth angular interval, $\Delta\phi$, was provided in the program to allow for the relatively small $\Delta\phi$ intervals required for adequate resolution of large values of θ without having an excessive amount of detail at small values ot θ. The option used to provide an increase in $\Delta\phi$ at small values of θ is defined by the program input. No properties of the gas are used to provide a variation as in the Δs interval. The logic in the option provides a constant value of cos θ times the solid angle. This tends to equally weight the heat transfer for each line of sight from a geometric standpoint.

In using this option the input variable

$$\text{TANGLE} = \sin\theta \cos\theta \, \Delta\theta \, \Delta\phi \qquad (2.18)$$

is specified along with a limiting minimum value of $\Delta\phi$. Then for each value of θ a value of $\Delta\phi$ is calculated, the number of $\Delta\phi$ increments required is computed, and the $\Delta\phi$ is recalculated to give an integral number of increments in the required ϕ range. This results in a $\Delta\phi$ equal to or slightly less than that which would be predicted by equation (2.18). If the $\Delta\phi$ computed is less than the input $\Delta\phi$, then the input $\Delta\phi$ is used in place of the computed value.

Using this option, the minimum value of computed $\Delta\phi$ would be reached at $\theta = 45^{\circ}$, with larger values of $\Delta\phi$ being computed at other values of θ. Not enough experience has been gained with this option to comment on its effect on the precision of the calculation, but it is likely that it may be necessary to modify the procedure used if significant radiation is received at large values of θ. In these cases, a procedure to maintain a constant solid angle would be better. Then $\Delta\phi$ at large values of θ would be fixed by the minimum input value.

Spectral Interval - $\Delta\omega$

Various methods of averaging the absorption coefficients over larger spectral intervals were experimented with in an attempt to find a method for using a larger spectral integration interval, $\Delta\omega$. All of the experiments were conducted on a special modification of the program, with no provision being made in the standard program for averaging over larger intervals. The modifications included (1) a section in the ACDATA subroutine to average the absorption coefficient and line density data and (2) revisions to the MODL3A subroutine to integrate the carbon absorption coefficient and blackbody function. The experience which has been gained with averaging should be used only as a guide, and a typical line of sight

for a particular problem should be tested before an averaging method is selected for integration.

In general, the carbon oxides due to their narrow spectral range are most sensitive to increasing spectral intervals. Water vapor radiation can usually be integrated with wavenumber intervals up to 100 cm^{-1} using a simple arithmetic average of k and 1/d. There has been some experience (reference 16) to indicate that results with errors of less than one percent can be obtained by using the values of k, 1/d, and the blackbody function at 100 cm^{-1} intervals in the standard program with no averaging at all. In the case of carbon particles, large spectral intervals may be used since the optical depth is linear with k,and it can be approximated as a gray body over large intervals. In one example of a low altitude exhaust plume with high temperatures near the outer boundary due to afterburning and a moderate carbon concentration (one percent mass fraction), integration with a spectral interval of 8000 cm^{-1} (using an integrated arithmetic average of k) was only 2.23 percent greater than the result using a 25 cm^{-1} integration interval.

Two difficulties are encountered in using a simple arithmetic average for gases. First, the values of k are generally high where 1/d is low and vice versa. This results in an average value for 1/d which is larger than it should be. As a result the optical depth tends to stay at the linear limit longer than it should, and the square-root limit is higher than it should be. The second difficulty is that, for very large spectral intervals, the non-gray behavior of the gaseous radiation tends to produce an average absorption coefficient which is not properly weighted to be used with the integrated blackbody function. A solution to these difficulties was attempted by weighting the absorption

coefficients by the blackbody function (assuming low absorption) and by weighting the value of 1/d by the value of k.

In order to weight 1/d, it was assumed that the case to be considered was in the square-root limit so the desired result was the proper value for $\sqrt{k(1/d)}$. The equations used for this averaging method for the interval ω_1 to ω_2 are

$$1/\bar{d} = \left[\sum_{\omega_1}^{\omega_2} \sqrt{k(1/d)}\ B_{\omega}^{o}\ \Delta\omega \Big/ \sum_{\omega_1}^{\omega_2} \sqrt{k}\ B_{\omega}^{o}\ \Delta\omega \right]^2 \qquad (2.19)$$

When this method was applied to the typical lines of sight used in the scaling study (Figures 5 through 7) excellent results were obtained as shown in Table 2.2. In all cases except the hydrocarbon plume without carbon particles results with intervals of 400 to 800 cm^{-1} were accurate enough to be used for many applications. Additional examination of the cause for the large errors in the hydrocarbon plume might reveal a better averaging method for this case.

The use of large spectral intervals can be extremely useful in making parametric studies, such as determining which location receives peak heating or what geometric step size is best to use, even if the estimated error is larger than is desired in the final result.

TABLE 2.2

RESULTS OF EXPERIMENTS WITH LARGE SPECTRAL

INTEGRATION INTERVALS

Line of Sight	$\Delta\omega$ cm^{-1}	Predicted Radiance Watts/cm^2- ster.	Error Percent
H-1, Figure 5	25	4.978	-
(No carbon)	100	5.061	1.66
	400	6.014	20.8
	800	6.404	28.6
	1600	7.178	44.2
	8000	14.85	198.3
(With 1 percent	25	18.612	-
carbon)	100	18.599	0.07
	400	18.837	1.20
	800	19.013	2.15
	1600	19.227	3.30
	8000	19.172	3.01
S-II, Figure 6	25	1.407	-
	100	1.411	0.29
	400	1.449	3.02
	800	1.512	7.44
	1600	1.495	6.27
	8000	2.096	48.96
J-2, Figure 7	25	0.1511	-
	100	0.1513	0.13
	400	0.1536	1.65
	800	0.1569	3.84
	1600	0.1622	7.35
	8000	0.1701	12.57

Note: All cases integrated from 1000 to 9000 cm^{-1}.

3 EFFECT OF SCALE ON GASEOUS RADIATION

The scaling to be considered is the geometric scaling of similar systems. This condition applied to rocket exhaust plumes is illustrated below.

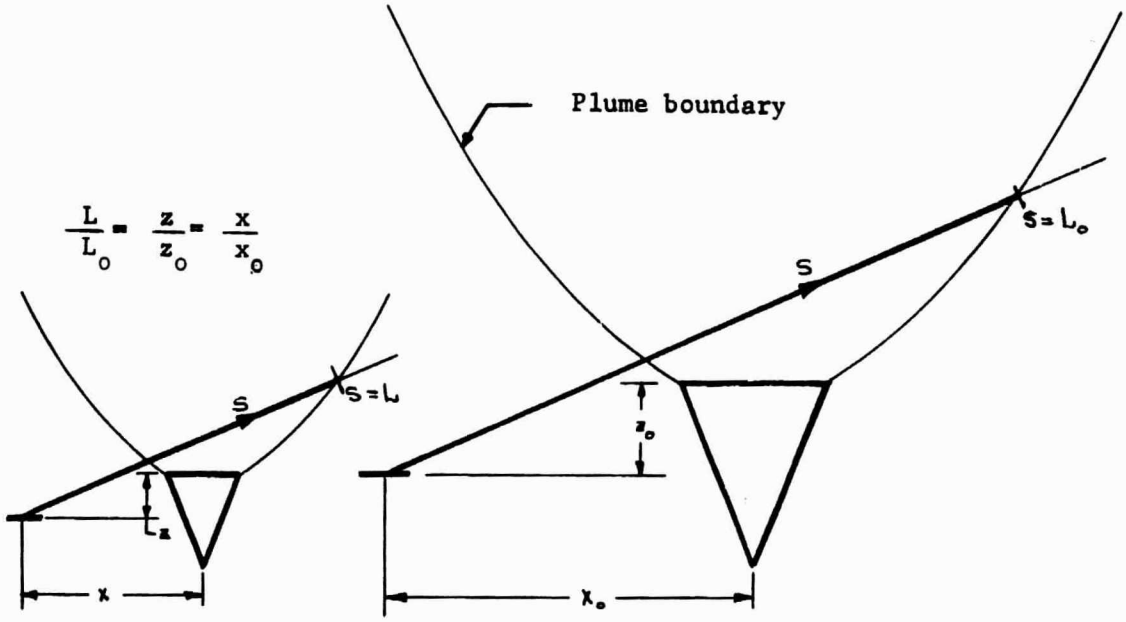

Illustration of geometric similarity

It is necessary that the spatial distribution of gas properties as well as the location and orientation of the observer be geometrically similar. In the illustration and in the subsequent discussion for a single line of sight, the characteristic length is taken as the distance along a line of sight from the observer to the farthest gas boundary, but in an integrated heat transfer calculation any characteristic dimension such as the engine exit diameter could be used.

An evaluation of the effect of scale on gaseous radiation is helpful in understanding the fundamentals of radiation characteristics in typical problems, and it is also desirable when there is not sufficient information about the gas properties to accurately predict radiation analytically. Even if no scaling laws can be developed, the knowledge of the sensitivity of gaseous radiation to scale can be a great help in making an engineering evaluation of the methods to be used in an estimating radiation heat rransfer. In order to properly present the effects of scale, the dependency of gaseous radiation on scale will first be analyzed before the computed scale effects in representative problems are reviewed.

Dependency of Gaseous Radiation on Scale

In order to provide a basis for evaluating the effect of scale, a simplified analysis will be examined to illustrate what effects may be expected in ideal limiting cases. This analysis will be carried out using the band model relations presented in Section 2, so the spectral values noted are actually averages over small intervals.

If equation 2.1 is taken for a single line of sight at a single spectral interval, the radiance is

$$N_\omega = \int_0^L -N_\omega^o \, (dT/ds)ds \tag{3.1}$$

which can be integrated for gases with constant properties to yield

$$N_\omega = N_\omega^o(1 - T(\omega,L)) \tag{3.2}$$

In this simplified form, the effect of transmissivity on the resulting radiance is clearly shown, and an evaluation of the transmission characteristics can be directly related to the resulting effect on radiance.

The transmissivity is expressed as a function of an optical depth, D.

$$T(\omega,L) = \exp(-D(\omega,L)) \tag{3.3}$$

and the dependence of the optical depth on the path length L varies with the radiation characteristics and partial pressure, p_i, of the radiating gas. In the weak line limit, the optical depth of a homogeneous layer is

$$D^*_\omega = k_\omega(p_i, T)\, L \tag{3.4}$$

if the absorption coefficient k_ω is taken as a function of pressure and temperature. But in the usual case the absorption coefficient is defined at standard temperature, T_o, and pressure, p_o, and then corrected for the actual conditions.

$$D^*_\omega = k_\omega(STP)\,\frac{To}{T}\,\frac{p_i}{p_o}\,L \tag{3.5}$$

In the following discussion, the absorption coefficient k_ω will be taken at standard conditions and the concentration - path - length parameter will be termed u. With these stipulations, equation 3.5 becomes

$$D^*_\omega = k_\omega u \tag{3.6}$$

In the weak line limit, D^*_ω is small compared to the ratio of average line half width, b, to line spacing, d, and $D_\omega = D^*_\omega$. For this case,

$$T_\omega = \exp(-k_\omega u) \tag{3.7}$$

so the optical depth is directly proportional to the path length, u. But when the radiation is not in the weak line limit, the effects of the collision and Doppler broadened curves of growth need to be considered.

For the case of collision broadening, the band model representation of the optical depth is

$$D_{c\omega} = k_\omega u / (1 + k_\omega u / 4a_{c\omega})^{\frac{1}{2}} \qquad (3.8)$$

where a_c is the collision broadened fine structure parameter (b_c/d_ω). This expression provides a transition from the linear region where $k_\omega u << a_{c\omega}$ and $D_{c\omega}$ approaches $k_\omega u$ to the square root region where $k_\omega u >> a_{c\omega}$ and $D_{c\omega}$ approaches $(4\, a_{c\omega} k_\omega u)^{\frac{1}{2}}$. Figure 4 represents an illustration of the behavior of this function for water vapor with varying total pressures. As the total pressure decreases, the collision broadened half-width, b_c, decreases in proportion and the curves of growth reach the square root limit at lower values of the path length, u.

As collision broadened optical depth decreases with decreasing pressure, Doppler broadening becomes significant. The representation for the Doppler broadened optical depth is

$$D_{D_\omega} = 1.7\, a_{D_\omega} \ln \left(1 + \left(\frac{k_\omega u}{1.7\, a_{D\omega}}\right)^2\right)^{\frac{1}{2}} \qquad (3.9)$$

Where $a_{D\omega}$ is the Doppler broadened fine structure parameter $(b_{D\omega}/d_\omega)$. As with collision broadening, this expression reduces the $D_{D\omega} \approx k_\omega u$ when $k_\omega u << a_{D_\omega}$, but since the Doppler half-width, b_{D_ω}, is not a function of pressure there is a single curve for Doppler broadening for a given temperature and wavenumber.

Although this representation in Figure 4 is for a particular temperature and spectral position, it illustrates the general condition that Doppler broadening is primarily significant at low pressures. The method of combining the Doppler and collision broadened optical depths into an overall optical depth was presented in Table 2.1, but an approximate method is to neglect the smaller of the two depths as long as they differ by a factor of 3 or more.

In examining the theoretical limits of scaling only isothermal isobaric gases will be considered. Attempting anything more from an analytical standpoint usually leads to development of simplified methods of radiation calculation in which gas property information is required. The two cases to be considered are, first, a transparent gas in both the linear and square root limits, and second, an opaque gas.

In the transparent gas case, a direct relation for scaling can be obtained if the optical depth ($D(\omega,L)$) is small compared to unity. For this case, equation 3.3 becomes

$$T(\omega,L) \simeq 1-D(\omega,L) \tag{3.10}$$

and equation 3.2 reduces to

$$N_\omega = N^o_\omega \; D(\omega,L) \tag{3.11}$$

If the entire spectral region of interest is in the linear limit ($D_\omega = k_\omega u$), then the radiance may be scaled to some reference condition (subscript o) and integrated to yield

$$N/N_o = L/L_o \tag{3.12}$$

A similar approach for radiation in the square-root region ($D_\omega = \sqrt{4a_{c\omega} k_\omega u}$) yields

$$N/N_o = (L/L_o)^{1/2} \tag{3.13}$$

But this is not a limiting case for long path lengths as the linear case is for small path lengths. If the pressure is low enough to allow the assumption that D_ω is much less than unity for the square-root region (refer to Figure 4 for illustration), Doppler broadening is likely to be significant which would cause a variation in the sensitivity to scale.

From this first simplified scaling example, it appears that there could be some cases in which radiance is proportional to the geometric scale if the path length, u, is small enough to put the significant portions of the spectra in the linear region and if the optical depth, $k_\omega u$, is small compared to unity. It is a simple matter to estimate the path length required for these conditions for a particular spectral position. For example, using the conditions illustrated in Figure 4,

$$ku/(4b_c/d) = 0.0375L$$

If it is required that this be less than 0.1 to stay near the linear region then

$$L \leq 2.67 \text{ cm}$$

Although a simple representation such as this is not representative of the entire spectrum, it does illustrate the very short path lengths which would be required for a full scale geometry in order for it to be scaled using equation 3.12.

The second limiting case to be considered is applicable to conditions in which the transmissivity approaches zero. For example, if the optical depth

is 3, the transmissivity is only 0.05, and at values of D greater than 3, the radiance rapidly approaches the blackbody value. In this case

$$N_\omega = N_\omega^o \tag{3.14}$$

for an isothermal gas, and scale has no effect on the radiance. But the conditions required for this case must be carefully examined.

For a pure gaseous species, a large size gas body is required to have all lines of sight through the gas opaque over all spectral regions in which the gas may radiate, so it is unlikely that a scale model would fulfill this condition. Although rocket engines using kerosene as fuel have carbon particles in sufficient quantity to cause the gas to be opaque under some operating conditions, the variations caused by the nonisothermal effects cause variations with scale as will be demonstrated in the following examples.

Computed Scale Effects

Since the limiting cases which have been described are not representative of typical problems, a study was made to determine how the behavior of radiation for typical conditions in rocket exhaust plumes would compare with the ideal cases with the possibility that scaling could be carried out with only a small sacrifice in accuracy.

The typical problems evaluated included plumes from rocket engines using both oxygen/kerosene and oxygen/hydrogen propellants. The cases of oxygen/kerosene propellants included both low altitude (afterburning) and high altitude conditions. For the oxygen/hydrogen cases, the Rocketdyne J-2 engine plume (76.8 in exit diameter) was used. In one of these cases the line of sight was through an impingement zone between plumes on the Saturn S-II stage while two others were chosen through the undisturbed high altitude plume.

In each case the radiance ratio, N/No, was computed along with its derivative, $d(\ln(N/N_o)) / d(\ln(L/L_o))$. over a wide range of scaling conditions. Typical results are presented in Figures 5 through 8. Only one case is presented for a oxygen/kerosene plumes since it presents the typical condition that scale effects are extremely dependent on the carbon concentration, and one of the J-2 lines of sight was also omitted since the radiance was so low it did not appear to be significant.

The behavior of the hydrocarbon plume without carbon is influenced by strong carbon dioxide absorption. As the plume grows larger, more of the carbon dioxide radiation which is emitted from the plume occurs in the cooler outer boundary of the plume. With the addition of carbon, this characteristic influences the entire spectrum until the hotter regions of the plume are effectively masked, and the radiance decreases with increasing scale. The carbon also causes the radiation at very small scales to closely approach the linear limit.

In the case of the typical S-II line of sight (Figure 6), the radiance gradually approaches the linear limit at very small scales and is very close to a square-root variation at scales greater than one. On the J-2 line of sight in Figure 7, the region from which most of the radiation is emitted is at a lower pressure than for the S-II, so the approach to the linear limit is not as rapid.

The radiance derivatives presented in Figure 8 indicate the rather uniform behavior of the gaseous plumes compared with those containing carbon particles. With the drastic effect the carbon particles have on the scaling and the lack of reliable estimates of the carbon concentration, it appears that no reasonsble estimate of scale effects can be made for oxygen/kerosene exhaust plumes.

The more uniform behavior of the scaling derivatives for the oxygen/hydrogen exhaust plumes appears to hold more promise for achieving a suitable scaling estimate. The problem still remains that the values of the scaling derivatives cannot be assessed precisely without gas property data, but the relatively small difference in the scaling derivatives indicates that it is not too sensitive to property variations. Therefore, useful scaling estimates may be possible over small ranges in scale using derivatives calculate from approximate gas property data.

4 RADIOMETER MEASUREMENTS OF A J-2 ENGINE

Measurements were made of a Rocketdyne J-2 engine operating under simulated altitude conditions in the J-4 test cell at AEDC. The measurements were made using a Hayes Model FF-1 radiometer. The description of this test will include the test configuration, the radiometer calibration procedure, the results obtained, and an evaluation of the results including comparisons with predicted results.

Test Configurations

The engine was mounted vertically pointing downward in the J-4 test cell at AEDC. There was a space of approximately 6 inches between the exit plane of the inoperative engine and the top of the diffuser entrance. The radiometer was mounted on top of the air chamber around the diffuser entrance as shown in Figure 9. Mounting of the radiometer allowed it to pivot to various positions across the engine exit plane.

The Hayes FF-1 radiometer has a square detector and aperture with no optics to give a uniform square field of a view 8.1 milliradians on a side, with the total field of view including vignetting area 15.6 milliradians on a side. Operating console for the radiometer was located in an instrumentation house adjacent to the test cell and was connected to AEDC instrumentation lines at this point.

The radiometer case was equipped with a nitrogren purge for this test, but evidence of water in the radiometer housing indicated that either the purge was not working satisfactorily or that water spray was used in the cell when the purge was not on.

The conditions in the test cell for the instrument and its operation were poor and could not have been improved significantly without interfering with the engine test effort or redesigning the radiometer for improved protection and ease of alignment and calibration.

Radiometer Calibration

The radiometer was checked for spectral response in the laboratory and then calibrated on the test stand intermittently during the test.

The purpose of the laboratory calibration was to determine the spectral response of the radiometer so the relative sensitivity to the blackbody calibration source and the water vapor radiation could be evaluated. The radiometer detector is a Barnes Engineering thermistor with a KRS-5 window. A comparison of the measured spectral response and published data (reference 17) for the same detector is shown in Figure 9. The agreement between the two sets of data is excellent over the range covered, so the published data was used at longer wavelengths where experimental data could not be obtained due to low radiance levels of the available sources.

With this data, the range of response to blackbody radiation in the 1 to 10u region was 83 to 85 percent for temperatures of 900 to 1300 ^{o}K which were normally used in calibration. The integrated response to the anticipated water vapor radiation over the same spectral interval was 85 to 86 percent depending upon the engine mixture ratio. Because of this near equality in sensitivity between the blackbody and water vapor radiation no correction was made for this effect in reducing the data.

The radiometer calibration on the engine test stand was performed by holding a blackbody source close enough to the radiometer to entirely fill the field of view. The calibration data listed with the other measurement results in Table 4.1 was consistent throughout the test except for two occasions. In the first instance, beginning after Test 08, the sensitivity of the radiometer appeared to increase, but later the same month it was found that the blackbody control was not working properly. Because of the uncertainty in the calibration data and its lack of agreement with the rest of the data, the October calibrations were not used in data reduction. The second time the calibration became erratic was at the end of the test. During the calibration after test 30 there was an apparent decrease in sensitivity of the radiometer. At this time, the radiometer output was becoming very noisy and after test 32 complete failure occured. The apparent cause of the failure was water damage inside the radiometer which may have been occuring over several tests. Therefore, the data taken after the February 5, 1968 calibration is considered unreliable.

If the instances of poor calibration results described above are omitted, the remaining calibration data agree well as shown in Figure 11.

Test Results

The results represent data on two different engine configurations. Tests 06 through 13 were on an engine configuration which, in a production version, would have had a nominal nozzle stagnation pressure of 702 psia at an overall mixture ratio of 5.5. Subsequent tests were made after modifications were made to uprate the engine to a configuration which would have a nozzle stagnation pressure of 718 psia at an overall mixture ratio of 5.5. After these tests on the J-2 engine, measurements were attempted on a J-2S engine, but no useful data were obtained.

TABLE 4.1

DATA FOR RADIOMETER MEASUREMENTS OF A J-2 ENGINE
IN THE J-4 TEST CELL AT AEDC

Date	Test Number	Time Sec.	Nozzle Stagnation Press-psia	Mixture Ratio O_2/H_2	Radiometer Viewing Angle	Signal Level mv	Calibration Temperature °K	Apparent Radiance Watts/cm^2-ster
8-22-67	CAL					16.5	973	1.62
8-22-67	06A	12	617	5.0	0°	11.1		1.13
		28	705	5.5		19.9		1.87
	06B	4.5	552	4.5		6.8		0.77
	06C	21	622	5.0		9.9		1.03
		28	704	5.5		17.5		1.67
	06D	5	539	4.5		4.2		0.55
9-7-67	CAL					16.5	973	1.62
9-12-67	08A	11	540	4.5	0°	7.0		0.79
		29	692	5.5		19.6		1.85
	08B	4.5	541	4.5		7.0		0.79
	08C	12	613	5.0		11.0		1.13
		29	694	5.5		17.6		1.68
	08D	4.5	543	4.5		6.8		0.77
10-2-67	CAL				Left	20.5	973	1.62
					10.8°	20	973	1.62
						29	1073	2.39
						43	1173	3.42
10-11-67	11A	10	636	5.0	Left	10.6		1.09
		29	709	5.5	10.8°	17.9		1.71
10-12-67	CAL				Right	18	973	1.62
					10.8°	28.5	1073	2.39
						41	1173	3.42
10-17-67	12A	9	630	5.0	Right	10.1		1.05
		29	708	5.5	10.8°	16.9		1.62
10-23-67	CAL					20.5	973	1.62
						31.5	1073	2.39
						44.5	1173	3.42
10-24-67	13A	12	618	5.0	Right	12.6		1.26
		28	699	5.5	10.8°	21.5		2.01
	13B	4.5	607	5.0		10.8		1.11

Delay for blackbody repair and calibration and repair of radiometer.

TABLE 4.1 (Continued)

DATA FOR RADIOMETER MEASUREMENTS OF A J-2 ENGINE
IN THE J-4 TEST CELL AT AEDC

Date	Test Number	Time Sec.	Nozzle Stagnation Press-psia	Mixture Ratio O_2/H_2	Radiometer Viewing Angle	Signal Level mv	Calibration Temperature ^oK	Apparent Radiance Watts/cm^2-ster
12-20-67	CAL				0°	9.5	868	1.03
12-21-67	21A	6-10	663	5.0	0°	12.2		1.23
		29.5	757	5.57*		22.1		2.06
	21B	5-7	658	4.9		11.7		1.18
	21C	5-7	658	4.9		11.2		1.14
	21D	5-7	656			10.1		1.05
1-4-68	22A	7-11	646	5.0	0°	9.4		0.99
		29.5	732	5.62*		17.5		1.67
	22B	4-6	633	4.9		6.2		0.72
	22C	4-6	635	4.8		7.1		0.80
	22D	4-7	636	4.9		5.4		0.6[illegible]
1-9-68	CAL				0°	9.5	879	1.08
						16.5	977	1.65
						26.5	1086	2.51
						15.0	947	1.45
						15.5	956	1.51
						8.0	834	.87
						4.0	739	.54
1-10-68	23A	10-12	645	5.0	0°	9.6		1.01
		29.5	733	5.63*		18.0		1.71
	23B	6-7	631	4.9		8.1		0.88
	23C	6-7	630	4.9		6.5		0.75
	23D	6-7	628	4.9		4.9		0.61
1-16-68	24A	8-10	645	5.3	0°	8.9		0.95
		29.5	729	5.95*		16.4		1.58
	24B	4-7	564	4.6		3.9		0.52
1-19-68	CAL				Left 10.8°	17	968	1.59
						26.5	1069	2.36
						16	957	1.51
						8.5	842	0.91
1-23-68	25A	8-10	638	5.0	Left	11.5		1.17
		29.5	731	5.66*	10.8°	21.4		2.00
	25B	4-7	566	4.4		5.7		0.68
	25C	8-10	644	5.0		9.7		1.02
		20-30	728	5.68		17.9		1.71
	25D	4-7	566	4.4		4.2		0.55

TABLE 4.1 (Concluded)

DATA FOR RADIOMETER MEASUREMENTS OF A J-2 ENGINE IN THE J-4 TEST CELL AT AEDC

Date	Test Number	Time Sec.	Nozzle Stagnation Press-psia	Mixture Ratio O_2/H_2	Radiometer Viewing Angle	Signal Level mv	Calibration Temperature °K	Apparent Radiance Watts/cm^2-ster
1-29-68	CAL				Right	10	856	0.97
					10.8	17	966	1.57
						27	1068	2.35
						17	952	1.48
						10.5	866	1.02
1-30-68	26AA	20	569	4.5	Right	7.8		0.85
		29.5	728	5.63*	10.8°	23.1		2.15
2-5-68	CAL				Left	15.0	981	1.67
					21.5°	9.0	868	1.03
2-6-68	27A	12-16	647	5.0	Left	16.7		1.61
		22-32	732	5.5	21.5°	27.0		2.48
2-22-68	29A	5-7.5	638	5.0	Left	8.0		0.87
	B	5.5-7.5	641	5.0	21.5°	7.5		0.83
	C	5-7	637	5.0		7.1		0.80
	E	5-7	631	5.0		7.0		0.79
3-1-68	30A	6.5-7.5	631	5.0	Left 21.5°	9.5		1.00
3-7-68	CAL				0°	7.5	889	1.13
						14.0	1005	1.84
						23.0	1089	2.54
						28.5	1128	2.92
3-8-68	31A	20-30	622	5.1	0°	8.5		0.92
	B	11-12	643	5.2		8.0		0.87
		29.5	730	5.89*		14.5		1.42
3-14-68	32A	5-7	635	5.0	0°	8.2		0.89
		5-7	633	5.0		6.8		0.77

Radiometer removed because of excessive noise.

*The mixture ratio on these runs was determined from corrected reduced data for the engine thrust chamber. See text for methods of estimating remaining data.

During initial tests of the J-2S engine, it was run in an idle mode so the radiance was extremely low. By the time full power firings were attempted, the radiometer failed, and the measurement program was terminated.

The results obtained are presented in Table 4.1 with the calibration data and engine operating conditions. The pointing angle shown in the table is measured in a plane parallel to the engine exit between the estimated radiometer line of sight and a line from the radiometer pivot to the engine centerline.

Estimations of the engine operating conditions were made by evaluation of the engine data and estimates of the nominal engine operating conditions. The nozzle stagnation pressure (p_o) was estimated using the measured pressure at the injector end of the chamber (p_c) with corrections for the purge bias (15 psi) and combustor pressure loss.

$$p_o = (p_c - 15)0.9208 \qquad (4.1)$$

The correction for combustor loss was taken from the estimated value in the engine specification. Estimation of a representative mixture ratio was not so straightforward because of the various data and corrections involved in obtaining reduced mixture ratio data.

In several of the tests, the engine data were corrected and reduced at a particular time. These data included corrected propellant mass and volume flow rates, overall engine mixture ratio and the mixture ratio to the thrust chamber only. The thrust chamber mixture ratio obtained from this source are marked in Table 4.1. The mixture ratios for tests 21 through 26 and 31 which were not obtained from the reduced engine data were estimated using the reduced mixture ratio and

the indicated volume flow rates. The estimating method used was

$$O/F = (O/F)_R (Q_{O_2}/Q_{H_2})/Q_{O_2}/Q_{H_2})_a \qquad (4.2)$$

where

O/F = mixture ratio

$(O/F)_R$ = mixture ratio from corrected data

Q_{O2} = indicated oxygen volume flow

Q_{H2} = indicated hydrogen volume flow

a = subscript for indicated data used in computing corrected mixture ratio.

This estimate assumes that: (1) instrument corrections are a constant multiple of the indicated flow rate; (2) the mass flow of each propellant required by the turbo pump is a constant fraction of the total flow of each propellant; and (3) the propellant density remains constant during each test series. In tests where no reduced data were available, the mixture ratio is estimated to be either 4.5, 5.0, or 5.5 depending upon the nozzle stagnation pressure.

Representative data records are presented in Figure 12. Normally each test series consisted of several runs with one run about 30 seconds long with a shift in mixture ratio and the remaining runs about 7 seconds in length with a constant mixture ratio. The simulated altitude or cell pressure was usually stable after a brief starting transient as illustrated in Figure 12.

Evaluation of Results

The results which are considered to be reasonably reliable cover two viewing positions across the engine exit and two basic engine configurations. Results for the line of sight passing through the plume centerline are presented

in Figure 13a and those for the 10.8° view angle are presented in Figure 13b. Estimates of the radiation made using the band model parameters of reference 9 are also shown on the figures.

The gas properties for the analytical estimate were obtained using the method of characteristics program of reference 1 with equilibrium chemistry. In making the analytical estimates, no allowance was made for the turbopump exhaust gas which is injected into the nozzle through the wall of the nozzle bell. This gas is cool and very fuel rich so the absorption through the thin gas layer is probably negligible, but the displacement thickness may cause a slight increase in temperature and pressure by effectively reducing the area ratio.

The combined effect of mixture and chamber pressure on the test results plus the scatter in the test results makes a direct comparison of the data with the analytical estimates difficult. The dependence of the measured results on chamber pressure is comparable with that predicted analytically, judging by the shift caused by uprating the engine,with the greatest variation being caused by changes in mixture ratio and unaccounted for data scatter.

There appears to be a tendency for the results to decrease on successive runs in a test series at essentially the same operating conditions. The cause of this decrease was not determined, but the data from the first firing in each test series is probably the most reliable. If this assumption is made, then the difference between the measured and predicted radiance is quite large except in isolated instances such as Run Series 24. However, the uncertainties in gas property prediction and instrument operation prevent a conclusive statement as to the accuracy of the analytical prediction of radiation.

5 RECOMMENDATIONS

Recommendations for further work will be presented under three general headings: computer programs, radiation scaling, and radiation measurements.

Computer Programs

The success which was obtained using band model parameters averaged over larger spectral intervals promises considerable savings in computer time, or alternatively, a much more complete analysis. Further work should be done in this area to assure that the results obtained are valid for a wider variety of cases and determine if adjustments could be made to further improve the accuracy. In addition, program modifications to allow rapid evaluation of the integrated black-body function over large spectral intervals would be required to obtain maximum benefit from the larger spectral intervals.

Further work is also desirable in the mechanics of the program operation if an extensive heat transfer study is required for a new rocket vehicle. The program, as it now exists, is the result of some compromise and certain changes may be desired or even mandatory for future applications.

In order to simplify input for the program, it would be desirable to specify the position of shocks in the flow field along with the flow field input rather than with additional data as is now required. This change would require modification of the flow field prediction program (reference 3) as well as the radiation program. A better alternative would be the modification of the FLOWIN subroutine to add both shock points and blocking circles (simulating occlusions caused by structure) to an input tape along with the flow field properties.

If the program is to be used for new vehicles with engine arrangements other than a circular cluster, a modification of the flow field interpolation

subroutine would probably be desirable to take advantage of flow field symmetry to reduce the quantity of gas property data required.

Future application of the program to three-dimensional rocket exhaust will be severly handicapped if an accurate method of predicting gas properties in three-dimensional plumes is not developed. There is no program which adequately describes the exhaust plume from a cluster of highly underexpanded rocket nozzles under anything approaching realistic conditions.

Radiation Scaling

Radiation scaling without a knowledge of the gas properties cannot be shown to be accurate enough to be usable except in very restricted cases. However, it is possible that scaling is less sensitive to errors in estimated gas properties than an analytical radiation prediction would be. If a case develops in which the gas properties can be duplicated on a small scale but the properties cannot be well defined, then it would be worthwhile considering an evaluation of the sensitivity of scaling parameters to variations in the gas properties. This could be done by a parametric variation of gas properties and an evaluation of the effects on both scaling parameters and radiation estimates.

Radiation Measurements

The radiation measurement attempted on this program has shown that the accuracy of the analytical radiation measurements cannot be verified with a simple radiometer measurement of a rocket engine being tested for another purpose. If verification of the analytical estimates are to be made, it will be necessary to mount a major effort to find a representative experiment in which the gas properties are either well defined analytically or measurable, and then develop instrumentation suited to the particular test.

6 REFERENCES

1. Huffaker, R. M. and Dash, M. J.: A General Program for the Calculation of Radiation From an Inhomogeneous Nonisobaric, Nonisothermal Rocket Exhaust Plume. NASA TM X-53622, June 1967.

2. Delwadia, M., Reardon, J., and White, S. A.: A Three-Dimensional Radiation Program for the Saturn S-II Stage. Hayes International Corporation ER 1470, August 1967.

3. Prozan, R. J.: Development of a Method of Characteristics Solution for Supersonic Flow of an Ideal, Frozen or Equilibrium Reacting Gas Mixture. Lockheed Missiles and Space Co., Huntsville Research and Eng. Center, LMSC/HREC A782535-A, April 1966.

4. Study of the Spectral Emissivity of Carbon Particles Produced by a Rocket Motor. Final Report on Contract NAS8-11455, General Dynamics Corp., Convair Division, GD/C-DBE 66-006, May 1966.

5. Thompson, J. D.: A Study of Radiative Properties and Composition of the Turbine Exhaust Products in the F-1 Engine. Rocketdyne Division of NAA, R-6743, September 1966.

6. Study of the Radiation and Convection Environment of the Saturn V. Summary Report on Contract NAS8-11350, Hayes International Corporation, ER 1333, October 1966.

7. Study of Exhaust Plume Radiation Predictions - Interim Progress Report. Contract NAS8-11363, General Dynamics Corp., Convair Division, GDC-DBE-66-001, January 1966.

8. Study of Exhaust Plume Radiation Predictions - Interim Progress Report. Contract NAS8-11363, General Dynamics Corp., Convair Division, GDC-DBE-66-001a, February 1966.

9. Study of Exhaust Plume Radiation Predictions. Final Report on Contract NAS8-11363, General Dynamics Corp., Convair Division, GDC-DBE-66-017, December 1966.

10. Study of Exhaust Plume Radiation Predictions. Progress Report on Contract NAS8-21082, General Dynamics Corp., Convair Division, GDC-DBE-67-021, November 1967.

11. Krakow, B.; Babrov, H. J.; Maclay, G. J.; and Shabott, A. L.: Use of the Curtis-Godson Approximation in Calculations of Radiant Heating by Inhomogeneous Hot Gases. NASA TM X-53411, March 1966.

12. Malkmus, W.: J. Opt. Soc. Am., vol. 53, 1963, p. 951.

13. Malkmus, W.: J. Opt. Soc. Am., vol. 54, 1964, p. 751.

14. Malkmus, W.; and Thomson, A.: J. Quant Spectrosc. Rad. Transfer, vol. 2, 1962, p. 17.

15. Ludwig, C.; Ferriso, C.; and Acton, L.: High Temperature Spectra of the 15-μ Band of CO_2. General Dynamics Corp., Convair Division, GD/C-DBE65-024, November 1965.

16. White, S. A.; and Reardon, J. E.: Prediction of the Saturn S-II Base Radiation Environment. Hayes International Corporation ER 1469, August 1967.

17. Duncan, J.; Wolfe, W.; Oppel, G.; and Burn, J.: Infrared Horizon Sensors. University of Michigan Institute of Science and Technology, Report NAVSO P-2481, April 1965.

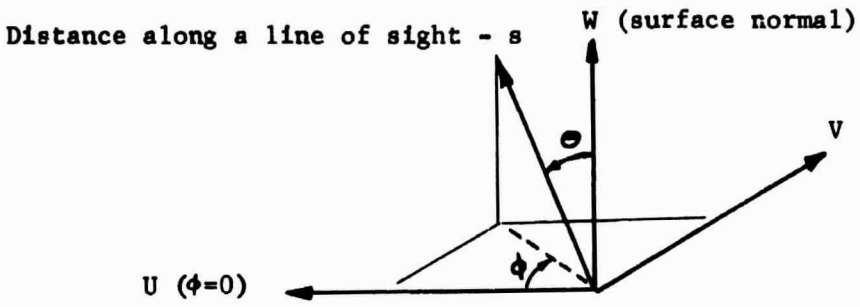

(a) Definition of spherical angles for radiant heat transfer integration.

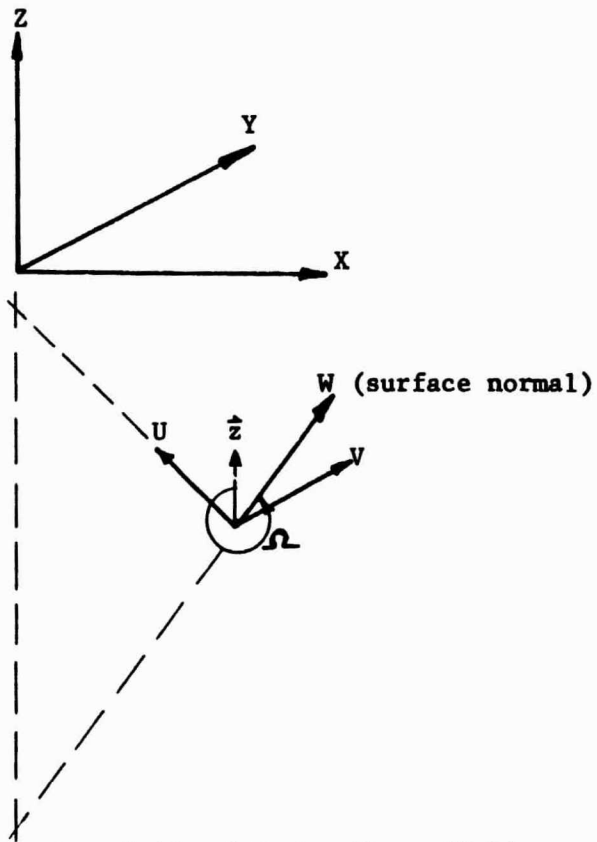

(b) Simplified alignment relation between the radiation calculation coordinate system and the gas body coordinate system.

Figure 1. Arrangement of the radiation program coordinate systems.

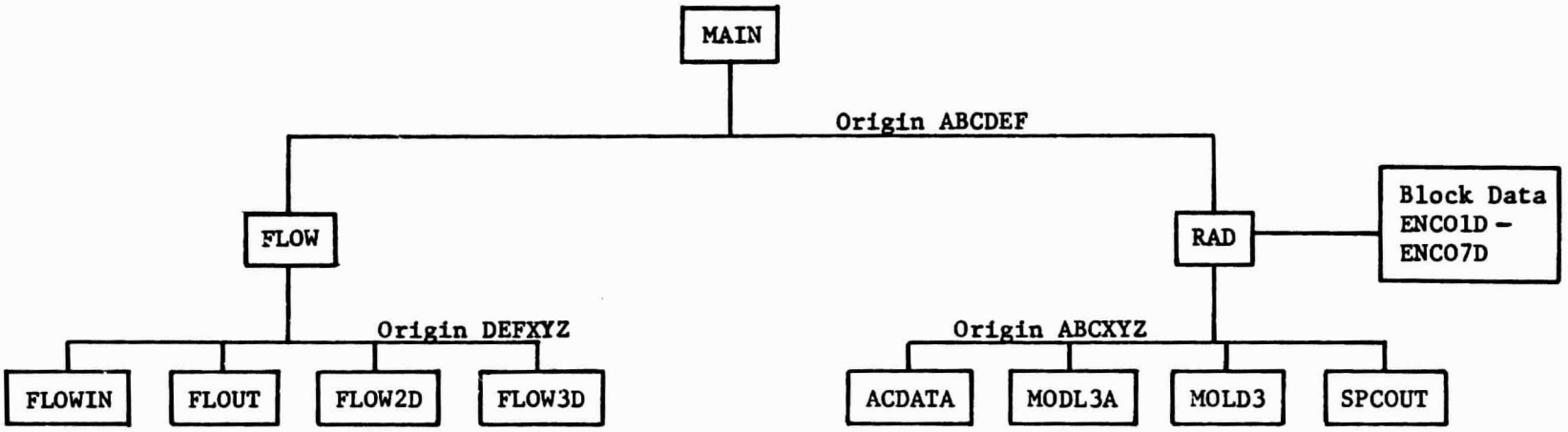

Subroutine	Function
MAIN	Program control.
FLOW	Controls FLOW subroutines.
FLOWIN	Initial flow field input and constituent identification
FLOUT	Output initial problem and geometry data.
FLOW2D	Prepare gas properties on lines of sight with axisymmetric property variations input.
FLOW3D	Prepare gas properties on lines of sight with three-dimensional property variations input.
RAD	Controls radiation subroutines.
ENCO1D-ENCO7D	Absorption coefficient and line density data.
ACDATA	Modify absorption coefficient data as required and output data to be used.
MODL3A	Calculate radiation using Model 3A.
MODL3	Calculate radiation using Model 3.
SPCOUT	Provide spectral output and plotting.

Figure 2. Radiation computer program arrangement.

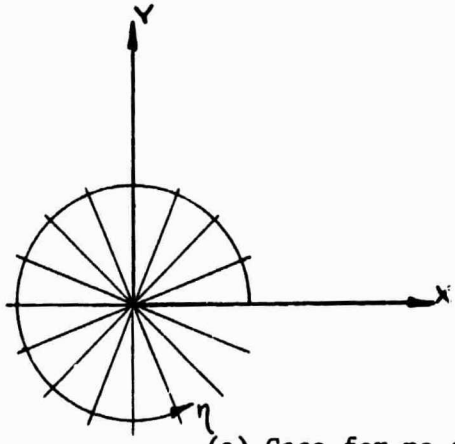

CTCD=0

HANG=360

η=0 to 360 (Maximum of 13 values is allowed)

(a) Case for no symmetry about the Z-axis.

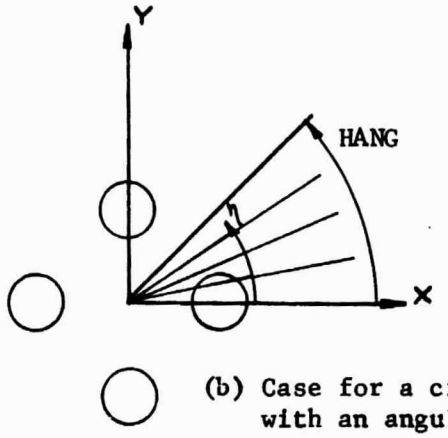

CTCD=0

HANG=360/2n where n is the number of engines

η=0 to HANG

(b) Case for a circular cluster of rocket engines with an angular spacing of 2(HANG).

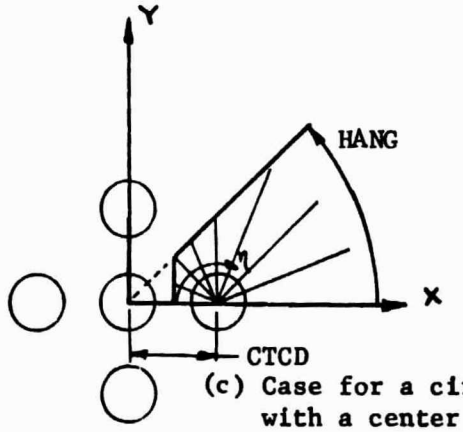

CTCD 0

HANG=360/2n

η=0 to 180

(c) Case for a circular cluster of rocket engines with a center engine. The center to outboard engine spacing is CTCD.

Figure 3. Illustration of loading options for three-dimensional property variations.

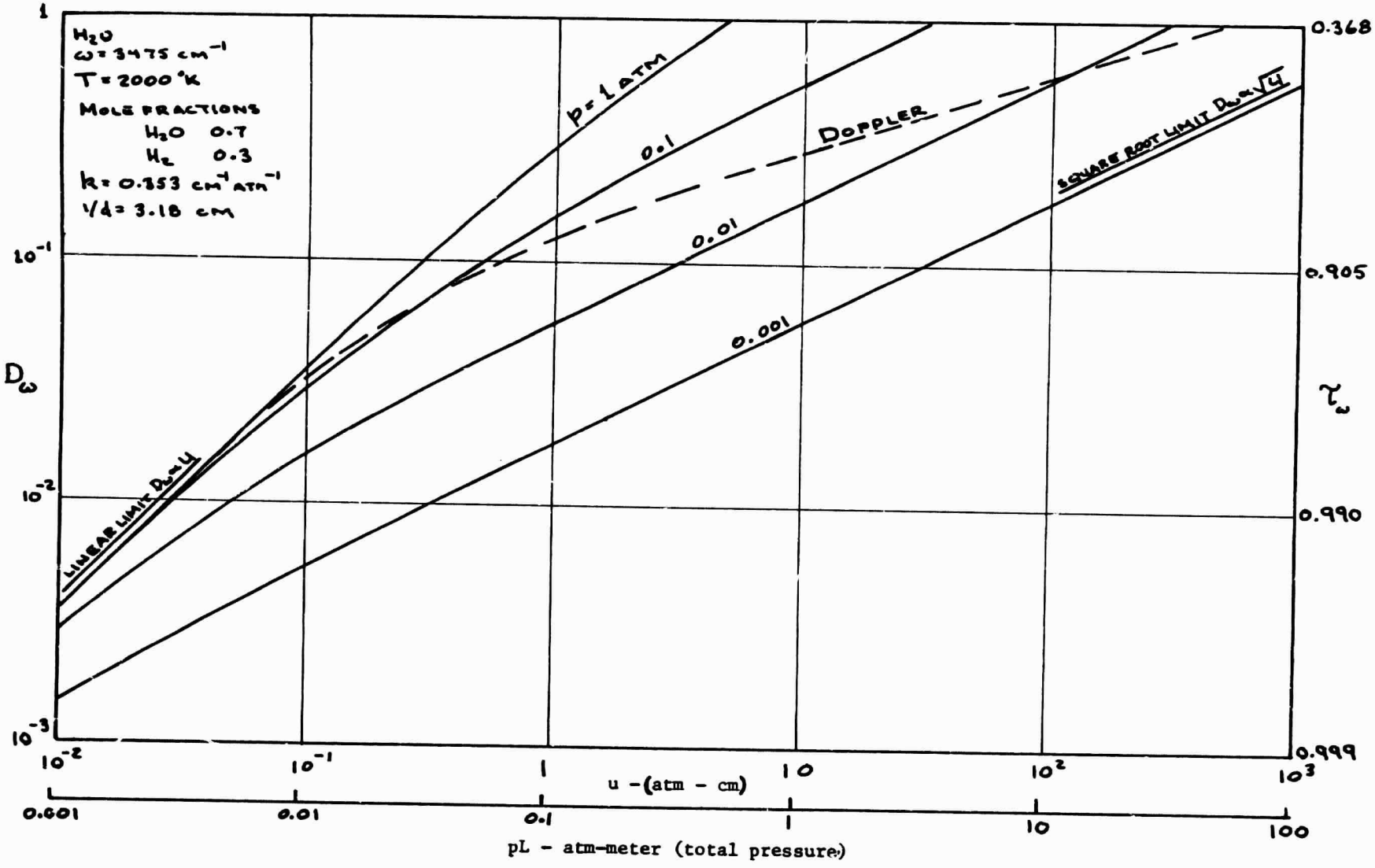

Figure 4. Example of Optical Depth Variations With Pressure and Path Length.

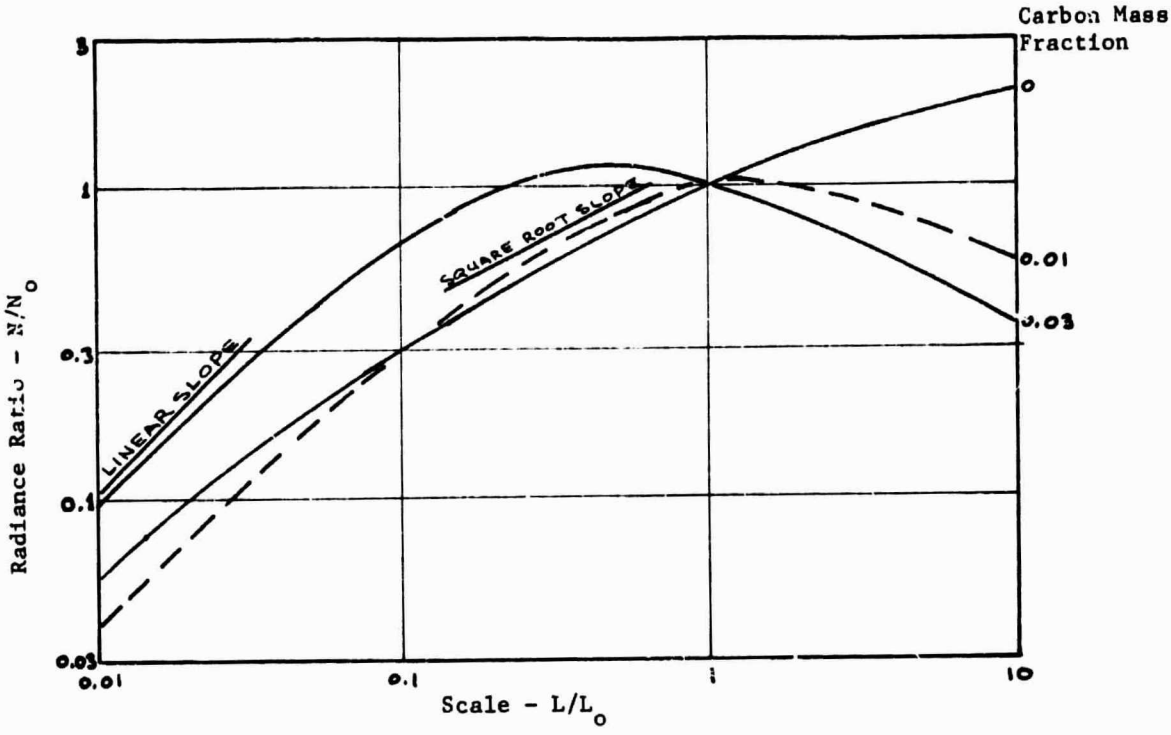

(a) Scale Effect on Radiance

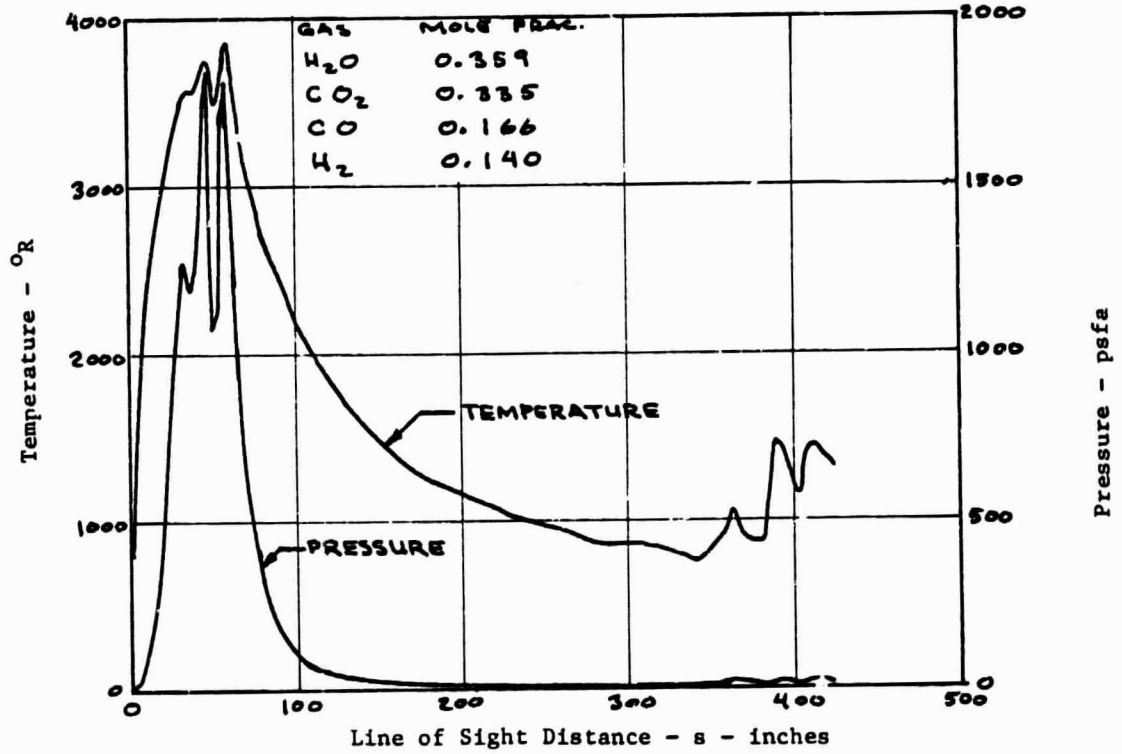

(b) Property Variation at Full Scale (L_o)

Carbon Mass Fraction	0	0.01	0.03
N_o Watts/cm^2 - ster	7.01	28.28	25.86

Figure 5. Scaling Results for a Typical Oxygen/Kerosene (H-1) Rocket Engine Exhaust.

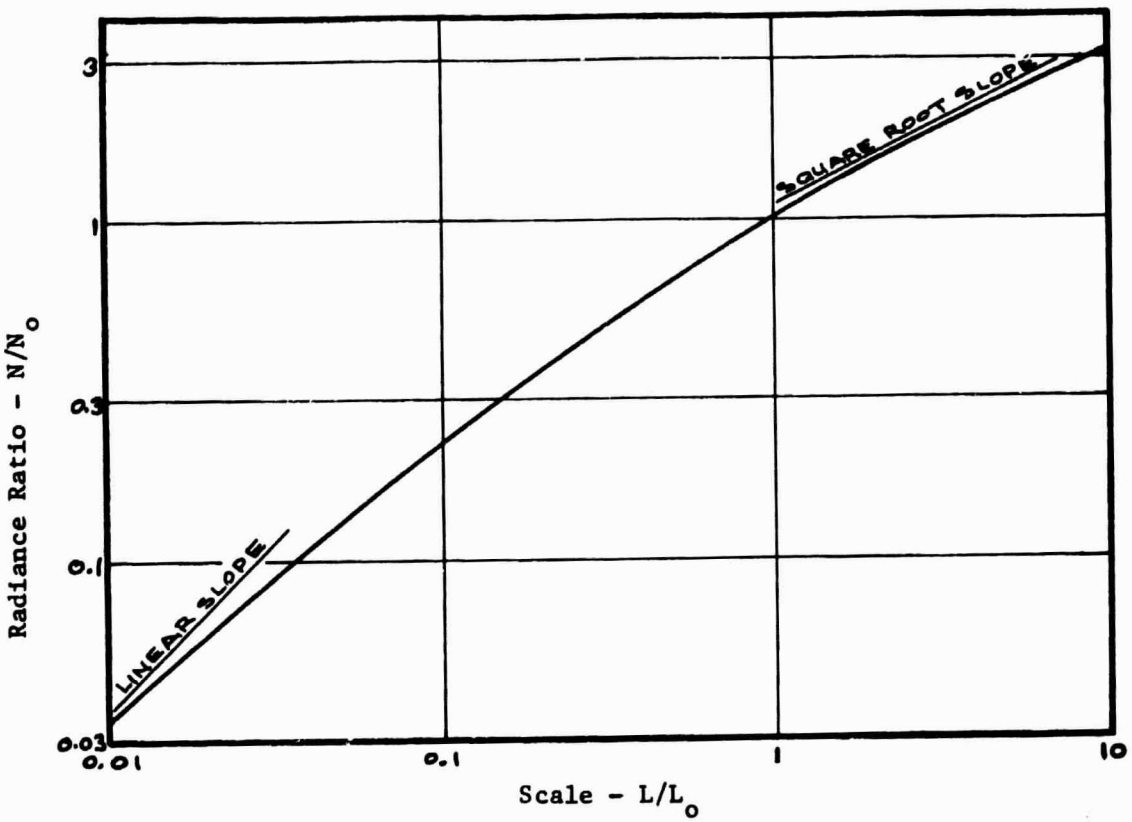

(a) Scale Effect on Radiance

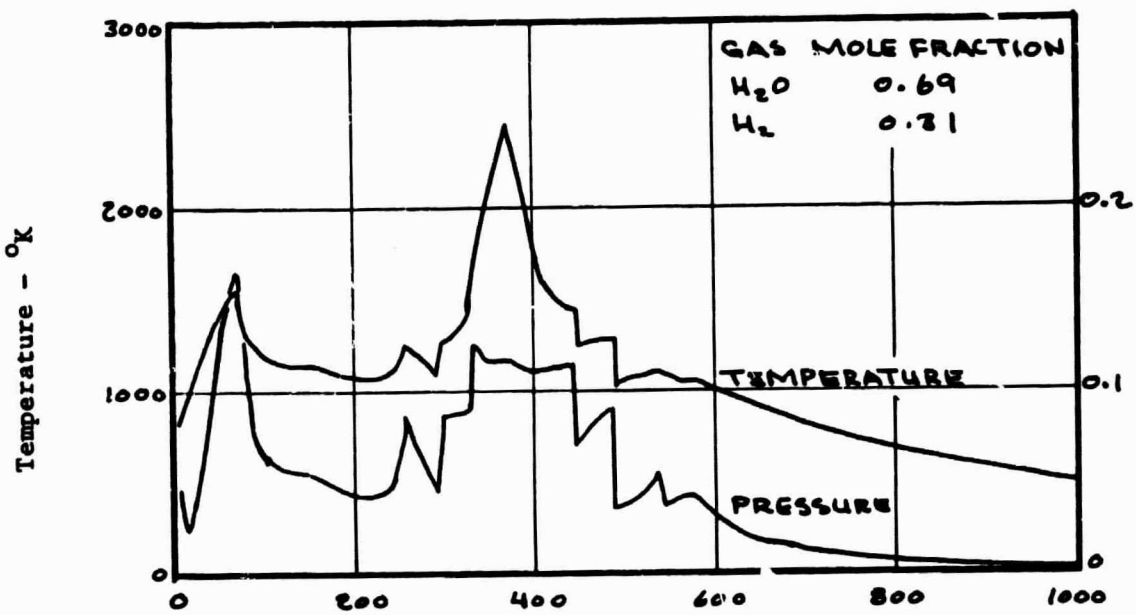

(b) Property Variation at Full Scale (L_o)

N_o = 1.56 watts/cm^2-ster.

Figure 6. Scaling Results for a Typical Oxygen/Hydrogen Plume from a Cluster of Engines (Saturn S-II Stage).

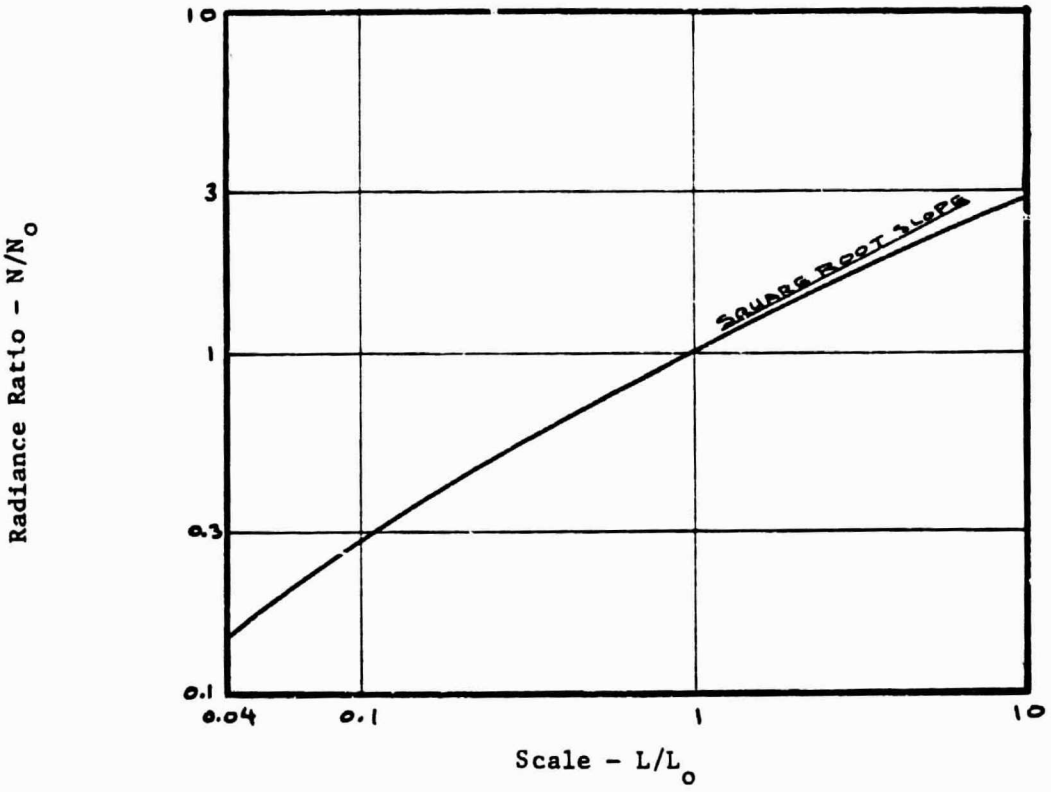

(a) Scale Effect on Radiance

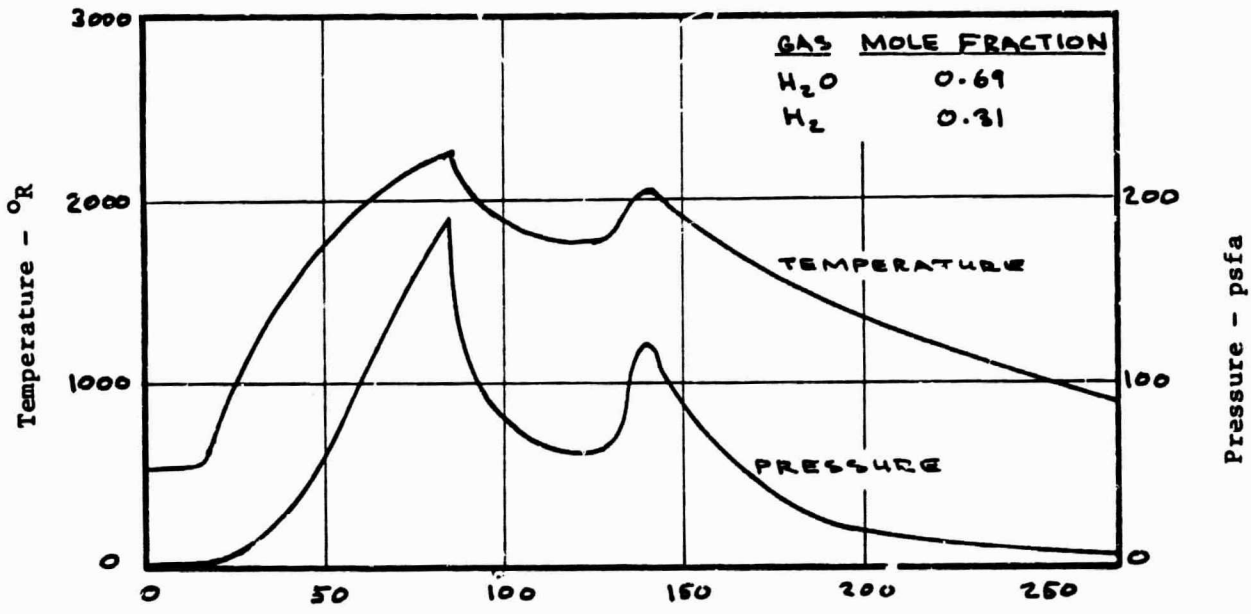

Line of Sight Distance - s - Inches

(b) Property Variation at Full Scale (L_o)

N_o = 0.174 watts/cm^2 - ster.

Figure 7. Scaling Results for a Typical Oxygen/Hydrogen (J-2) Rocket Engine Exhaust.

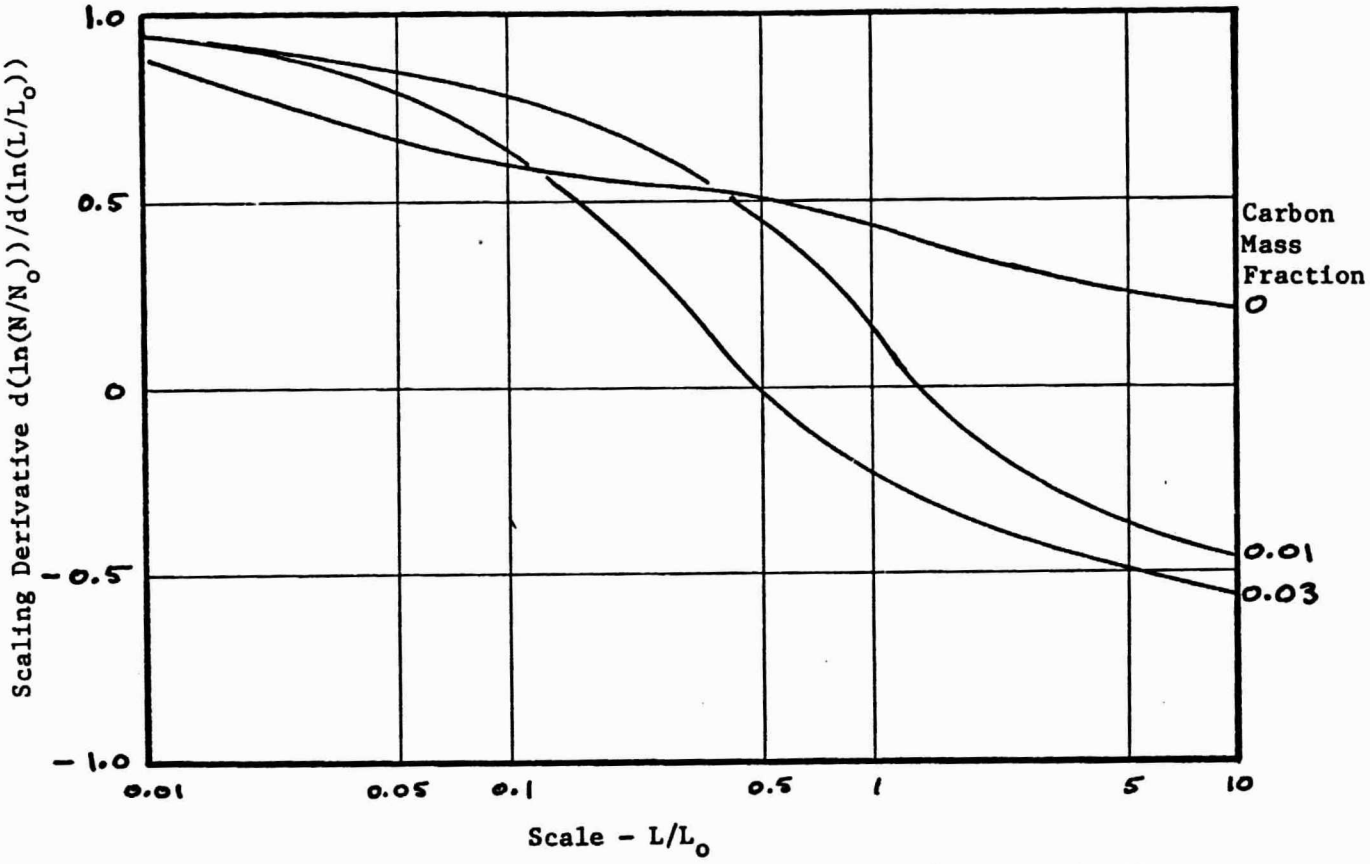

(a) Scaling Derivative Variation for the Oxygen/Kerosene (H-1) Exhaust Plume.

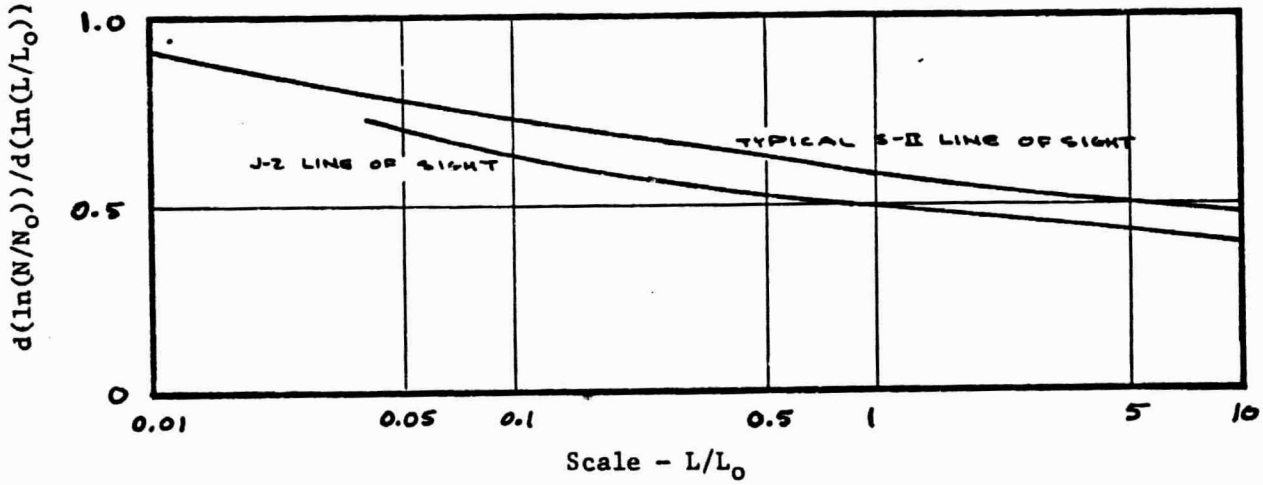

(b) Scaling Derivative Variation for the Oxygen/Hydrogen Exhaust Plumes.

Figure 8. Variations of Scaling Derivative for the Typical Conditions Studied.

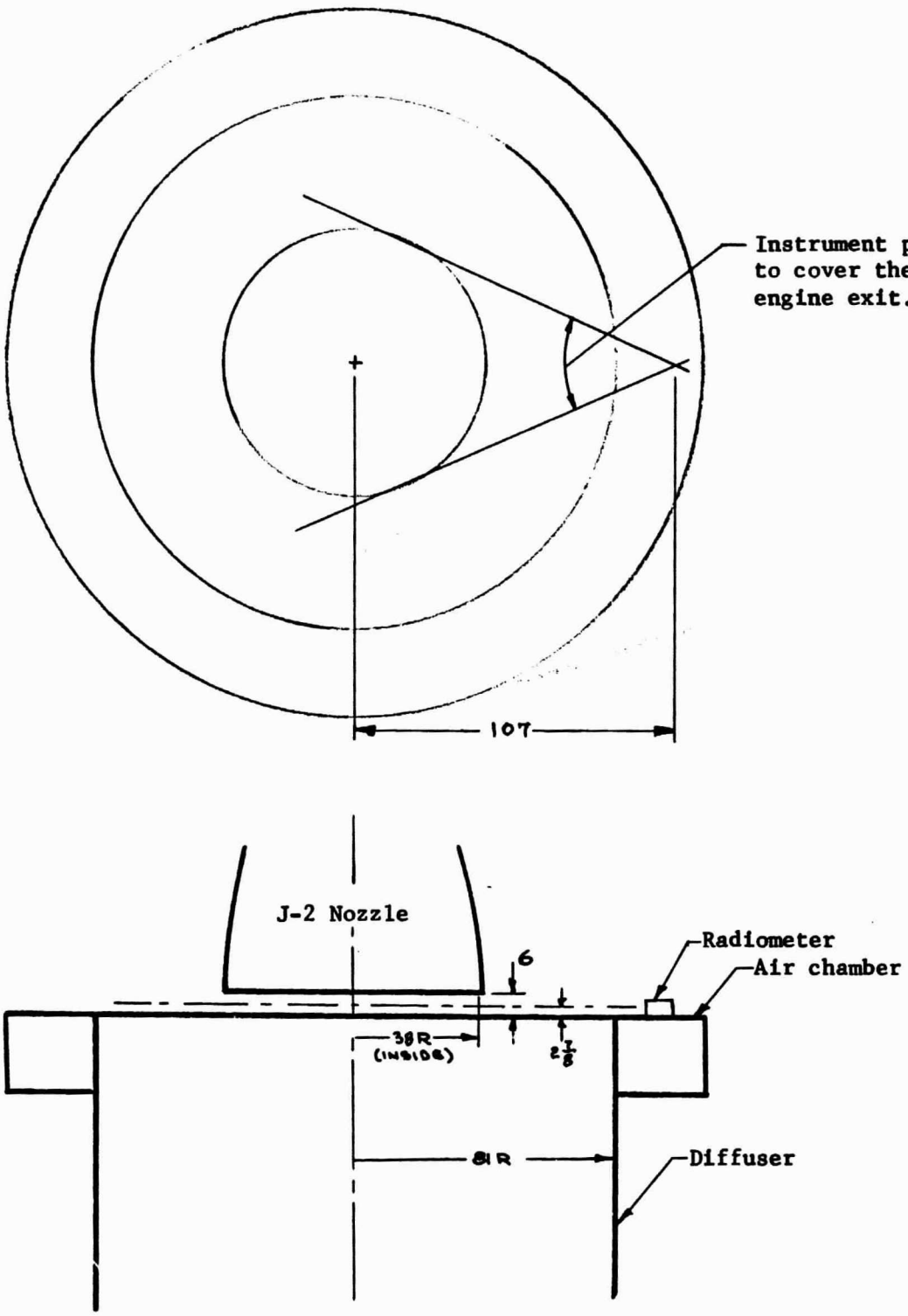

Figure 9. General arrangement of the J-2 engine in the J-4 Test Cell at AEDC.

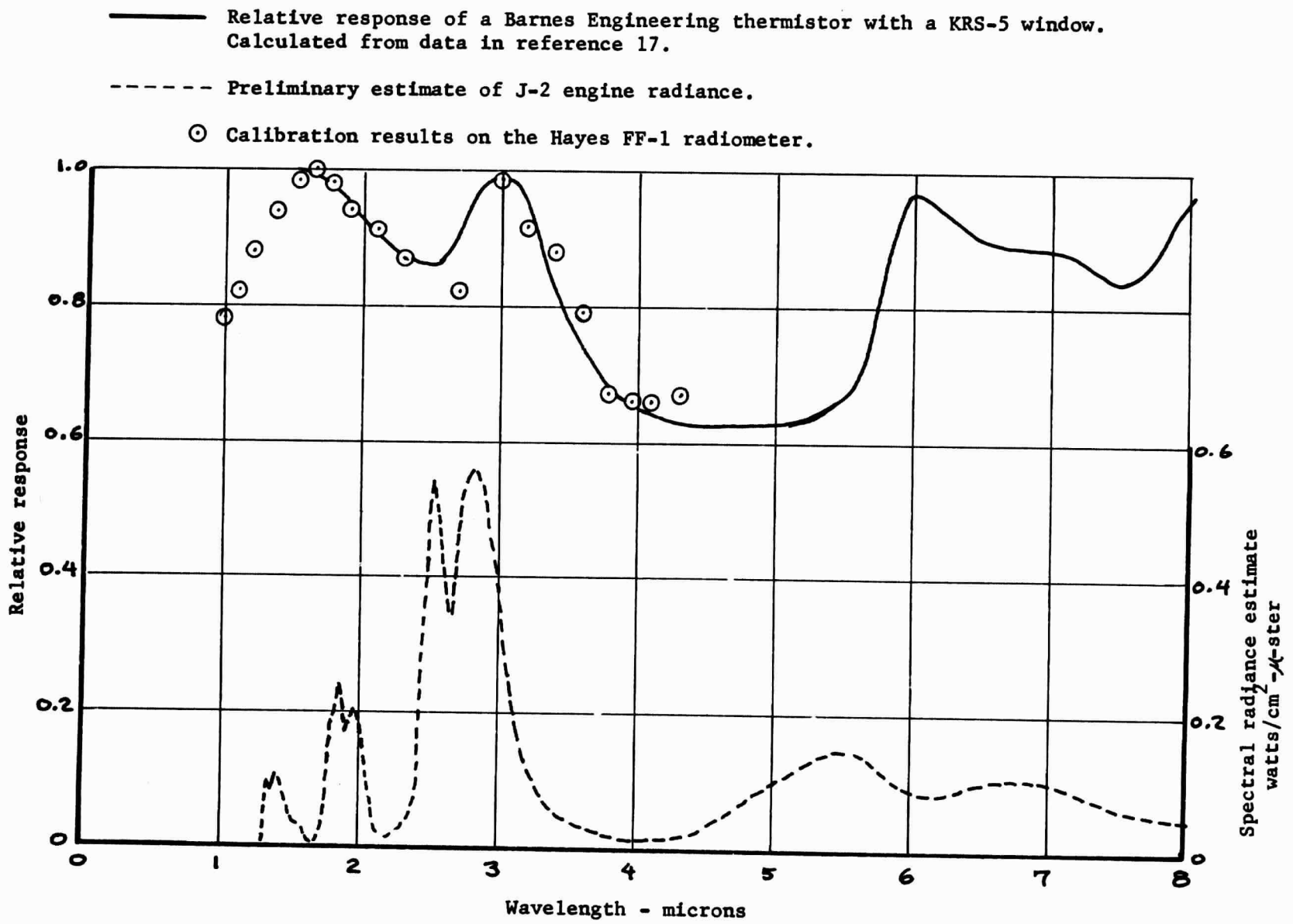

Figure 10. Spectral response of the Hayes FF-1 Radiometer.

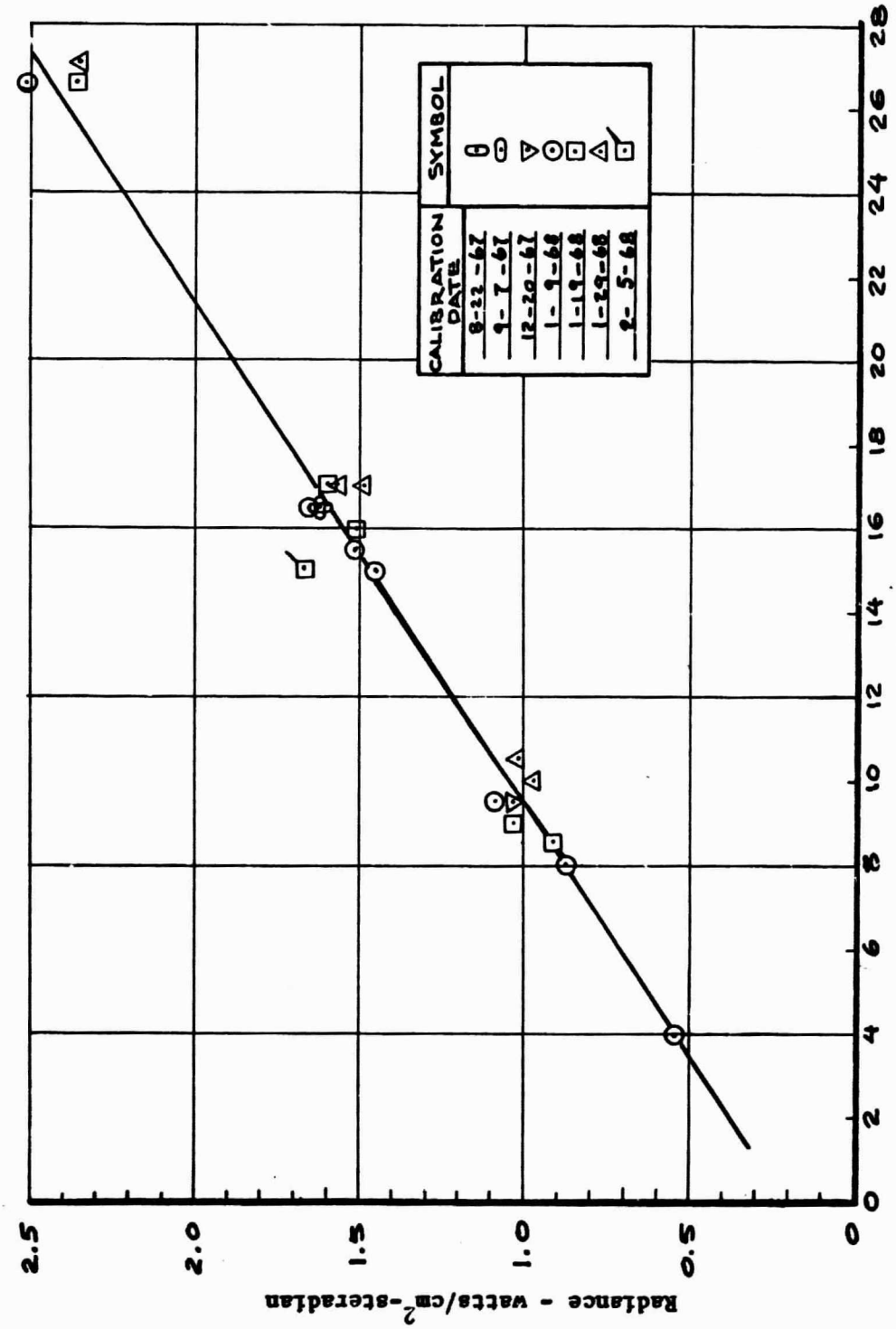

Figure 11. Radiometer calibration results.

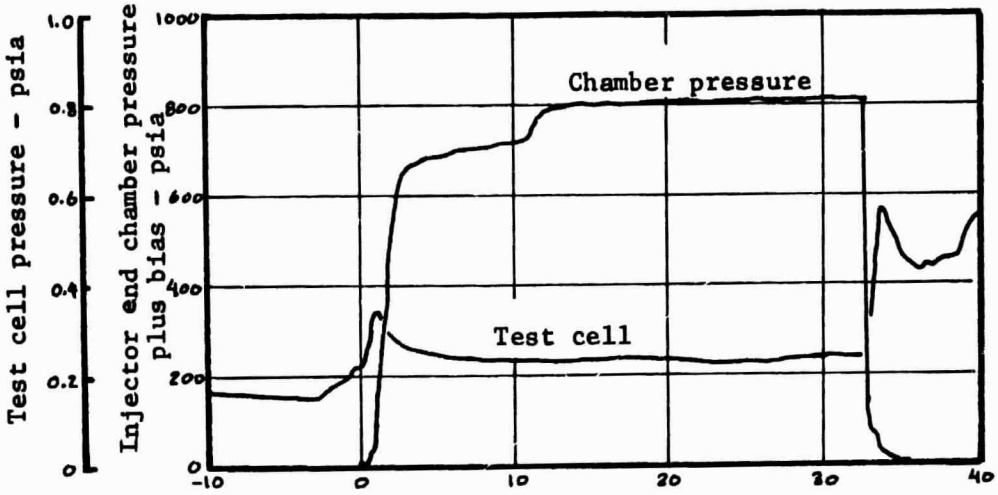

(a) Engine Chamber Pressure and Test Cell Pressure Records.

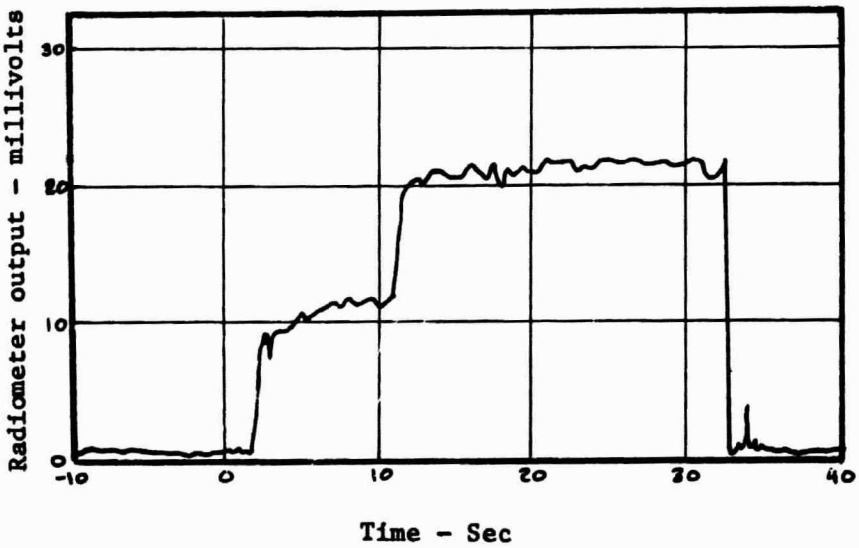

(b) Radiometer Output Record.

Figure 12. Typical Test Records from Computer Plot of Digitized Data for Test 25A.

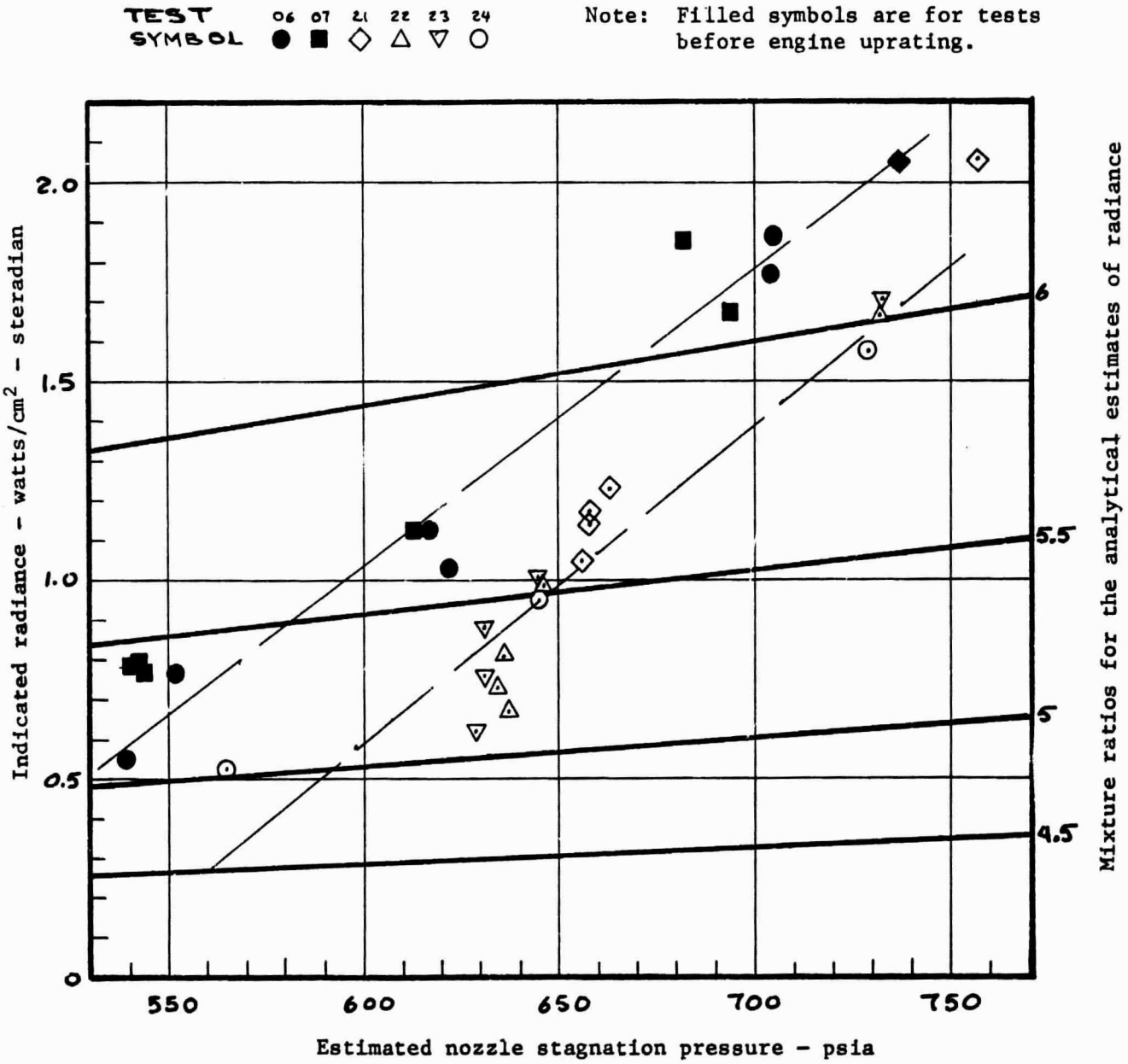

(a) Radiometer line of sight through the engine center line.

Figure 13. Test results.

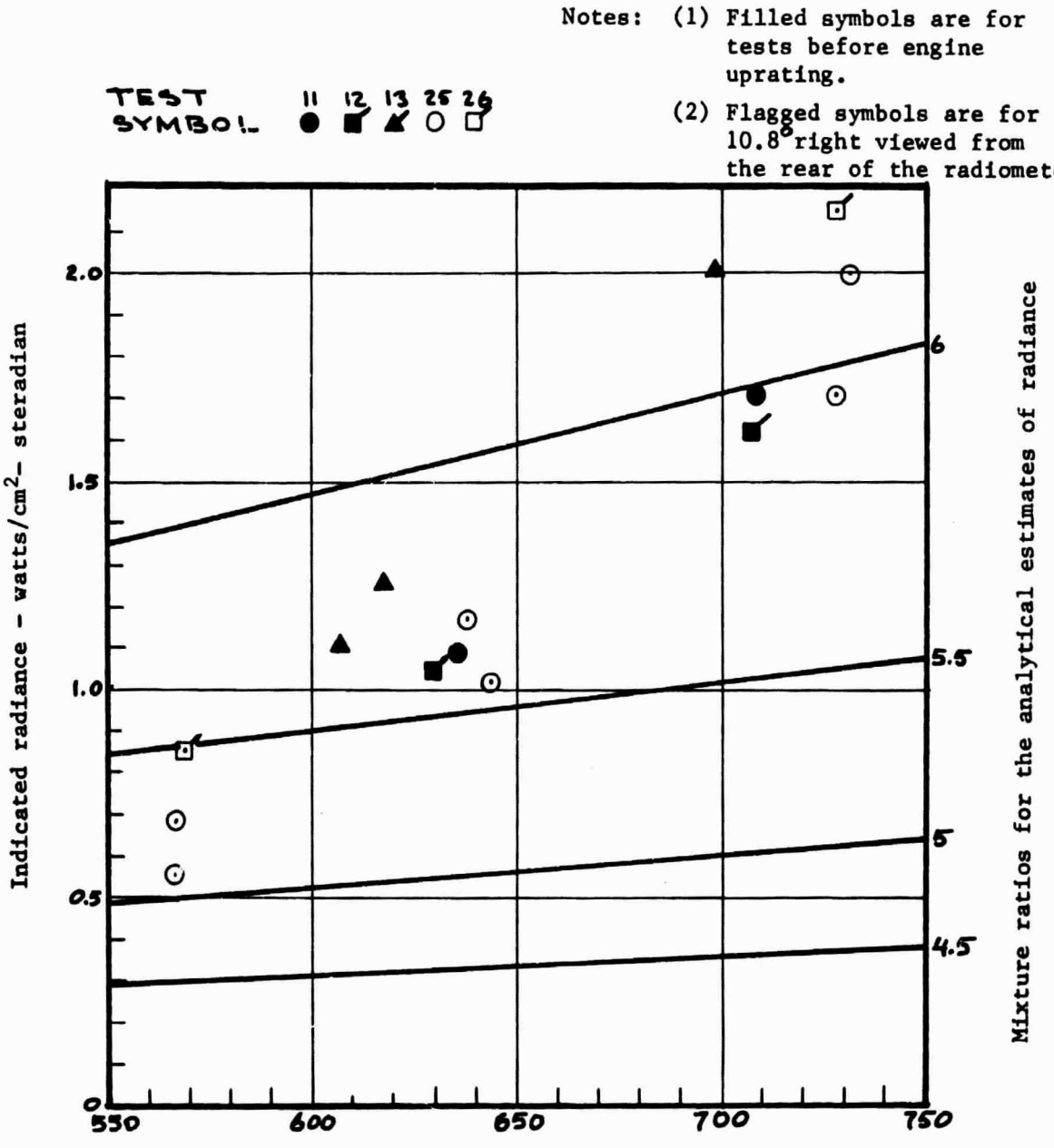

(b) Radiometer line of sight 10.8° from a line through the engine center line.

Figure 13. Test results (concluded)